MIMO Evolution Beyond 5G through Reconfigurable Intelligent Surfaces and Fluid Antenna Systems

Arman Shojaeifard, *Member, IEEE,* Kai-Kit Wong, *Fellow, IEEE,* Kin-Fai Tong, *Senior Member, IEEE,* Zhiyuan Chu, Alain Mourad, *Senior Member, IEEE,* Afshin Haghighat, *Senior Member, IEEE,* Ibrahim Hemadeh, *Member, IEEE,* Nhan Thanh Nguyen, *Member, IEEE,* Visa Tapio, *Member, IEEE,* and Markku Juntti, *Fellow, IEEE*

***Abstract*—With massive deployment, multiple-input multiple-output (MIMO) systems continue to take mobile communications to new heights but the ever-increasing demands mean that there is a need to look beyond MIMO and pursue the next disruptive technologies. Reconfigurable intelligent surface (RIS) is popularly considered as a candidate to provide the next generational leap. The first part of this paper provides an updated overview of the conventional reflection-based RIS technology which complements the existing literature to include *active* or *semi-active* RIS. Then we widen the scope to discuss the surface-wave assisted RIS that represents a different design dimension in utilizing metasurface technologies. This goes beyond being a passive reflector and can use the surface as an intelligent propagation medium for superb radio propagation efficiency. The third part of this paper turns the attention to fluid antenna, a novel antenna technology which enables a diverse form of reconfigurability that can combine with RIS for ultrahigh capacity, power efficiency and scalability. This paper concludes with a discussion of the potential synergies that can be exploited between MIMO, RIS and fluid antennas.**

***Index Terms*—6G, B5G, Emerging technologies, Fluid antennas, Reconfigurable intelligent surfaces, Surface waves.**

I. Introduction

A. Background

MOBILE communications today means more than simply untethered voice communications between two parties. It represents a multitude of services ranging from traditional ubiquitous access of multimedia communications to internet of everything (IoE) [1], [2], mobile edge computing [3], wireless power transfer [4] and etc. Cellular vehicle-to-everything (C-V2X) in fifth generation (5G) is also expected to revolutionize the automotive industry for years to come [5]. No matter how mobile networks have evolved, it has always been an effort to push the spectral efficiency and energy efficiency. The next generation, 6G, will look to support a myriad of new use cases and more ambitious key performance indicators (KPIs) [6].

During the past decades, numerous technology trends have been driving mobile communications forward. Amongst the various technologies, many consider multiple-input multiple-output (MIMO) by far as the most important breakthrough in recent history of mobile technology. The first edition of MIMO appeared in the patent by Paulraj and Kailath in 1994 [7], way ahead of its time. The interest however exploded only after the work of [8] and [9]. Foschini and Gans in [8] demonstrated that the channel capacity of MIMO increases linearly with the number of antennas at both ends. Concurrently, Tarokh *et al.* in [9] stunned the wireless world by their design criteria for space-time codes to exploit the spatial diversity. Shortly afterwards, Alamouti invented a genius $2 \times N$ space-time code which has now been included in many wireless standards [10]. The intuition that multipath can boost capacity was not easy to swallow at the time, and the benefits of MIMO were only formally characterized by introducing the notion of diversity and multiplexing tradeoff by Zheng and Tse in 2003 [11].

Furthermore, scattering in wireless communications means that MIMO can exploit the spatial signature of each user for multiple access. Research in multiuser MIMO began in 2000 [12], [13] and subsequently, the work by Vishwanath *et al.* in [14] and Spencer *et al.* in [15] sparked enormous interest and a paradigm shift from single-user MIMO to multiuser MIMO [16]. Using multiuser MIMO, the network capacity can scale with the number of users without additional bandwidth if the channel state information (CSI) is available at the transmitter side. A great deal of research was subsequently concentrated on the acquisition of CSI with limited feedback for multiuser precoding [17]. There have also been interesting developments when MIMO is to operate in the millimeter-wave (mmWave) band in which hybrid analogue-digital precoding can deliver high spectral efficiencies with less hardware cost and power consumption compared to fully-digital solutions [18]–[20].

Following 3GPP specifications work on full-dimension (FD) MIMO (FD-MIMO), in 5G, a large number of antennas at the base station (BS) is deployed. For 4G or long-term evolution (LTE), MIMO utilizes up to eight downlink and four uplink antennas, whereas 5G BSs today employ 64 or more antennas. The ultrahigh spatial selectivity of using a large number of BS antennas means that interference can be easily eliminated and this is achievable by applying a simple spatial matched filter [21], [22]. In fact, massive MIMO is still multiuser MIMO but comes with the virtue of simple precoding at the BS.

It goes without saying that our mobile technology has been

A. Shojaeifard, A. Mourad, A. Haghighat and I. Hemadeh are with InterDigital Communications Inc., UK/Canada.

K. K. Wong, K. F. Tong and Z. Chu are with the Department of Electronic and Electrical Engineering, University College London, UK.

M. Juntti, V. Tapio and N. T. Nguyen are with the University of Oulu, Oulu, Finland.

The work of K. Wong is supported in part by the Engineering and Physical Sciences Research Council (EPSRC) under grant EP/V052942/1.

Manuscript received September XX, 2021.

improving by a lot generation after generation. To satisfy the increasing data-rate requirements, mobile networks have had to move to higher frequency bands for larger bandwidths. The usage of higher frequency band unfortunately means reduced coverage performance in practice even in the presence of beamforming. Small cell technologies can deliver coverage enhancements by bringing remote radio heads (RRHs) closer to the user equipments (UEs) at the price of lofty deployment and operational (in particular energy) costs. Network densification does marry beautifully with edge computing which gives the UEs access to the supercomputing capability at the network edge [23], [24]. The prospect of bringing RRHs closer to the UEs seems bright, if only the energy footprint of BSs and RRHs can be minimized. Actually, a mmWave massive MIMO RRH in the form of a small cell is very power hungry, let alone the one with a computing server. On the other hand, relaying solutions for improving coverage, such as integrated access and backhaul (IAB), are also expensive, and infeasible for time-stringent applications. Repeaters are more cost-efficient, but in many scenarios increase interference levels.

B. Beyond MIMO Technologies

One red-hot idea to emulate the extraordinary performance of a massive MIMO 5G BS/RRH, but with a much smaller form factor and at a more affordable cost, is to deploy a surface of a large number of radiating elements in the environment. This essentially provides a large aperture to capture the radio waves from the BS (or UEs) and intelligently redirects them to the targeted UEs (or BS) by adapting the reflection coefficients of the elements. In this paper, this concept is referred to as reconfigurable intelligent surface (RIS) which is best introduced in the pioneering work [25]–[27].[1] A notable advantage of RIS is that it does not need power-hungry amplifiers to operate. With recent advances in low-power electronics, perpetual RIS operation can even be feasible [32]. The use of relatively cheap radiating elements also ensures a low hardware cost.

RIS represents an exciting, new paradigm of engineering the radio environment via carefully designed software-controlled elements (usually referred to as 'meta-atoms')[2] that can change their electromagnetic (EM) properties to suit communications. A recent report [33] demonstrates that it is possible to achieve a 21.7dBi antenna gain using an RIS with 256 2-bit elements at 2.3GHz, and a 19.1dBi antenna gain at 28.5GHz. RIS can even be used to perform digital modulation by adapting their reflection coefficients without using standard components such as mixers, and phase shifters, offering an opportunity to reduce the hardware complexity of wireless systems [29], [30].

Though the results are remarkable, RIS is an infrastructure-based approach and may require a large surface to be useful. There remains interest to incorporate a large number of antennas not only into the BS but the UE as well. Equipping a UE (e.g., a mobile phone) with multiple antennas is nevertheless difficult because of its limited space. Despite the fact that moving up the frequency bands has helped make the antenna smaller, a UE in 5G is not expected to have more than four antennas while the number of antennas at a BS has risen to as many as 64. To overcome the physical limits, metamaterials appear to be a promising technology and have been researched to allow small-sized antennas to be made [34], [35].[3]

Unfortunately, it is not just the antenna size that matters but also the separation between antennas. The common practice is that multiple antennas are deployed only if they have at least half a wavelength separation to guarantee sufficient diversity of the signals.[4] The 'half-λ' rule of thumb is suggested from the fact that in rich-scattering environments the spatial correlation between two signals is close to zero if they are half-wavelength apart [36]. It was shown in [37] that the 'half-λ' rule appears in the spacing of RIS elements as well to ensure performance.

Recently, a rather surprising result was presented in [38], [39] that enormous diversity could be obtained to reduce the outage probability even in a very small space if the position of an antenna can be changed. The concept is empowered by the emerging fluid antenna technology which represents any software-controllable fluidic, conductive structure that is able to alter its shape and position to reconfigure the gain, radiation pattern, operating frequency, polarization and other parameters [40]. In a wider sense, it may even include designs that involve no fluidic materials if they can mimic the agility [41], [42].

The term 'fluid antenna' was first used in [43] when distilled water and chemicals were proposed as potential materials for an antenna but reconfigurable fluid antennas emerged only in recent years, e.g., [44]–[49]. There is also an emerging idea to use pixels with RF switches for designing reconfigurable antennas and such idea could be an alternative version of 'fluid' antenna that can have delay-free switchable ports [41], [42]. A contemporary literature review for liquid-metal based 'fluid' antennas can be found in [50]. Note that seawater, albeit much less conductive than metal, has already been demonstrated a radiation efficiency of 70% by Mitsubishi Electric [51]. Also, a research group even developed an advanced saltwater-based antenna to achieve 360-degree beam-steering that works for frequencies between 334 to 488MHz [52], [53].

C. Vision and Scope

RIS has dominated the research of wireless communications in recent years and is tipped as a strong favourite to be a key enabling technology for 6G. The majority of RIS research has focused upon *passive reflection* but several variants have been proposed to enhance the capability of RIS utilizing reflection amplifiers [54], [55]. These recent developments motivate us to present an up-to-date review on active or semi-active RIS that is much less understood. As a matter of fact, intelligent surfaces represent more than an intelligent reflector and can include other reconfigurabilities such as acting as an intelligent

[1]The same concept may go by other names such as large intelligent surface [28] or programmable metasurface [29], [30]. A majority of research in the literature in fact refers to the concept as intelligent reflecting surface (IRS) but the recent industry specification group (ISG) by the European Standards Organisation ETSI has settled on the name RIS [31].

[2]In the literature, many names have been used. The terms 'atom', 'element' and 'cell' will be used interchangeably in this paper.

[3]Metamaterials are also particularly relevant to the RIS work as they may allow many more elements to be fitted in a given area for better performance.

[4]Diversity order measures the rate at which the error rate in communications drops against the log of the signal-to-noise ratio (SNR). It is well known that the diversity order will be M if we have M independent copies of the signal.

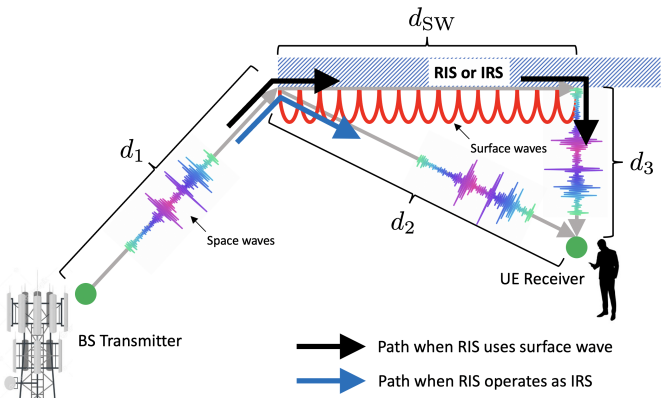

Fig. 1. A coarse illustration for path loss comparison when RIS operates in different modes. To highlight the advantage of using surface waves, only the path from the leftmost of the surface is traced but the radio waves arriving at different locations of the surface follow similarly.

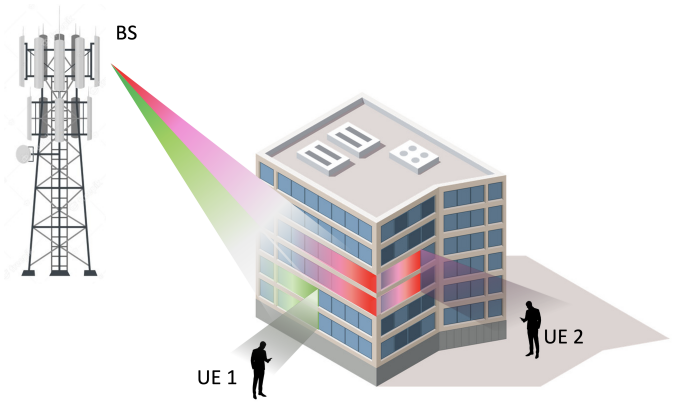

Fig. 2. Regionalized multiuser communications through RIS using a mixture of surface wave and space wave communications.

propagation medium. In [56], RIS was conceptualized to create smart radio environments using non-radiative, trapped surface wave propagation on surfaces in addition to bouncing space waves off surfaces as in reflection-based RIS. In particular, a surface-wave aided RIS can make radio waves glide along the surface before hopping off to reach the UEs, so as to:

- Enjoy a more favourable propagation condition for transmitting radio signals that has much less path loss. Specifically, the received power for surface wave is inversely proportional to the propagation distance, d, as compared to the squared distance in the case of space wave propagation [57]. In the far-field from an RIS, it is known that the received power, $P_r^{\rm RIS}$, satisfies $P_r^{\rm RIS} \propto \frac{1}{d_1^2 d_2^2}$ [58][5] while if surface wave is used on the RIS, see Fig. 1, the received power can become $P_r^{\text{s-RIS}} \propto \frac{1}{d_1^2 d_{\rm SW}^{\alpha} d_3^2}$, in which all the distances $d_{\rm SW}, d_1, d_2, d_3$ are defined in the figure and $d_2 = \sqrt{d_{\rm SW}^2 + d_3^2}$. Also, α denotes the path loss exponent for the surface wave and typically equals one for a standard surface. If a specially designed reconfigurable surface platform is used, it is even suggested that $\alpha \approx 0$ might be possible [59]. In that case and when the UE is close to the surface, i.e., $d_{\rm SW}, d_2 \gg d_3$, we have

$$P_r^{\text{s-RIS}} \propto \frac{1}{d_1^2 d_3^2} \gg P_r^{\rm RIS} \propto \frac{1}{d_1^2 d_2^2}. \tag{1}$$

- Simplify interference management. Surface waves adhere to the surface and radio waves away from the surface are drastically attenuated. Interference over the air is much less a problem and interference only matters if it is close to the surface. It means that multiuser communications on the same time-frequency resource can be achieved easily by regionalizing their signals, as shown in Fig. 2.

Evidently, such surface-wave aided RIS operates differently when compared to the mainstream effort that focuses primarily on passive RIS. This paper is devoted to review the relevant literature on where we are for RIS, discuss what it means to the design of mobile networks, and shed light on what potentials lie before us. In particular, we will also highlight the synergy between massive MIMO, RIS and fluid antennas.

[5]Note that an inverse square law is assumed here for simplicity. In practice, the exact path loss exponent will depend on the type of environments.

D. Organization

The rest of this paper is organized as follows. In Section II, we first review the recent literature of active and semi-active RIS. Then Section III covers the basics of surface-wave based RIS. In Section IV, our attention is then turned to fluid antennas. We will outline some latest fluid antenna technology and review some important theoretical results of fluid antenna systems. Most important of all, Section V presents our views on the potential of combining RISs and fluid antennas with MIMO for future-generation mobile communications. Finally, we provide our concluding remarks in Section VI.

II. Active and Semi-active RIS

Greatly motivated by low-cost electronics, the mainstream effort on intelligent surfaces so far focuses on the architecture that acts as a gigantic passive reflector to intelligently redirect the radio waves towards the intended UE receivers. An RIS is composed of many cells (or 'atoms'), each of which serves as a reflecting element with its reflection coefficient controllable via, e.g., changing the biasing voltage of a varactor diode. The current state-of-the-art is to use a microstrip or patch design for each reflecting cell which is best described in [60], [61]. In this section, we complement the existing work to discuss the active and semi-active RIS architectures. Compared to [62]–[64] which focus only on the optimization of semi-active RIS, we here analyze the capabilities of both active and passive RIS beamforming and discuss how RIS can combine with cell-free massive MIMO (CF mMIMO) for enhancing performance.

A. Passive Beamforming

In the physical layer, the optimization of RIS is generally equal to choosing the best phase values of the RIS cells since the amplitude responses of the cells cannot be independently adjusted and are usually assumed to be unity. Various system models have been considered for designing the RIS. In most

cases investigated, a multi-antenna BS is considered to transmit to the RIS which redirects the signals to one or many UEs. In the multiple-input single-output (MISO) case, the UE(s) is equipped with only a single antenna while the MIMO case refers to the situation where the UE(s) has multiple receiving antennas. In [65], Wu *et al.* studied the joint optimization of the BS beamforming and the passive reflection coefficients of the RIS for a single-UE system and the work was extended to the multiuser scenario in [66] where the total transmit power minimization problem was tackled subject to the UEs' signal-to-interference plus noise ratio (SINR) constraints. The same problem was then studied for the discrete phase-shift model in [67] and for the amplitude-varied phase-shift model in [68].

The optimization of RIS-assisted MIMO systems has also been studied in [69]–[72] and the work in [73] even addressed the multicell scenario. In the MIMO case where multi-stream transmission is supported, the RIS needs to properly balance the channel gains of the different spatial data streams.

The performance improvement of deploying multiple RISs is also characterized in [74], [75]. In [74], Yang *et al.* provided an approximate expression for the capacity in the asymptotic regime to examine the capacity scaling with the number of RISs. Wang *et al.* in [75] then combined RIS with mmWave communications and showed that the received signal power increases quadratically with the number of reflecting cells for both single RIS and multi-RIS cases. A common assumption in the capacity analysis of previous works is the adoption of Gaussian signaling; yet the input signals in practical systems use discrete constellations. This was also recently investigated in the context of RIS in [76]. Lastly, multiple RISs were also recently applied to cell-free networks in [77], [78].

B. Active/Semi-active Beamforming

With the introduction of reflection amplifiers [54], RIS can dramatically improve the beamforming gain. In this case, the amplitude response of each cell is no longer limited and can be independently controlled and optimized. In [79], Long *et al.* illustrated that active RIS achieves higher capacity than the conventional passive RIS. The gain of active RIS was further elaborated in [55], reporting up to 40dB gain in the received SNR when compared to the passive RIS system.

Though active RIS prevails, the use of reflection amplifiers adds to the cost of RIS considerably which may outweigh its benefit. A more attractive option is to have only a few active cells out of the many cells on the RIS. This idea was pursued recently in [62]–[64]. A fixed configuration was considered in [63], while [64] looked into dynamically selecting the number of active cells and their positions based on the propagation condition. The results in [63], [64] indicated that a few active cells were sufficient to obtain satisfactory performance gain. Another important benefit of this hybrid architecture is that the additional RF chains can aid channel estimation.

C. Power Consumption

An active RIS is neither a BS nor relay. The configurability of an active RIS is enabled through low-power electronic circuits (e.g., switches, varactors, tunnel diodes) [79]. In contrast, a BS or relay is equipped with sophisticated and power-hungry active electronic components such as analog-to-digital converters (ADCs), digital-to-analog converters (DACs), mixers, power amplifiers for transmission and low-noise amplifiers for reception. Advanced coding/decoding and signal processing techniques are also expected at the BS or relay which is not normally required by an active RIS. A surprising fact is that the computational complexity for optimizing an active RIS can be lower than that for optimizing a passive RIS. In particular, the complexity for optimizing the passive RIS coefficients is $O(M^6)$ [80], [81] while that for designing an active RIS needs only $O(M^{1.5}\log(\frac{2Mc}{\varepsilon}))$ [79] where M denotes the number of elements, c is a constant and ε is a prescribed accuracy.

The power consumption of an active or semi-active RIS is, however, higher compared to a passive one. It is shown that their power consumptions are, respectively, given by [79]

$$P_{\text{RIS}} = \begin{cases} MP_c & \text{if passive,} \\ M(P_c + P_{\text{DC}}) + P_{\text{out}}/\xi & \text{if active,} \\ MP_c + \tilde{M}P_{\text{DC}} + \tilde{P}_{\text{out}}/\xi & \text{if semi-active,} \end{cases} \tag{2}$$

where P_c is the power consumption of the switch and control circuit at each element, P_{DC} is the DC bias power consumption, P_{out} is the output power of the active RIS, $\xi \in (0, 1]$ is the amplifier efficiency, $\tilde{M}$ is the number of active elements in the semi-active RIS, and $\tilde{P}_{\text{out}}$ denotes the output power of the semi-active RIS. Note that in the semi-active RIS, $\tilde{M} \ll M$ and the output power is generally proportional to M.

D. Channel Estimation

Typically, RIS, regardless of passive, active or semi-active, requires the availability of CSI for the beamforming design. CSI acquisition for RIS scenarios nonetheless is very challenging and involves estimating two cascaded channels. Several channel estimation procedures have been proposed [82]–[85], some of which exploited the sparsity of the channel to simplify the estimation. Channel estimation can be done at the RIS if it has active receive processing chains [86]. However, typically, channel estimation is conducted at the BS mostly in the uplink direction [87]. The control network will need to send the used codebooks to the RIS so that training can be performed.

If identification of the individual component channels is required, a hybrid RIS architecture with receiver functionality (e.g., demodulation) will become necessary. Such an architecture was reported in [86]. Channel estimation for this hybrid architecture has further been studied in [88]–[90] while [91] even presented a hardware proof-of-concept.

E. RIS and CF mMIMO

While RIS seems perfect to work with MIMO at the BS for enhancing mobile coverage, mobile networks may see another transformation by letting a large number of access points (APs) serve as distributed BS antennas for super-massive coordinated beamforming in the cell-free architecture for accommodating many users on the same time-frequency resource block [92]–[95]. The integration of RIS and CF mMIMO has the potential to improve the network performance further [96], [97].

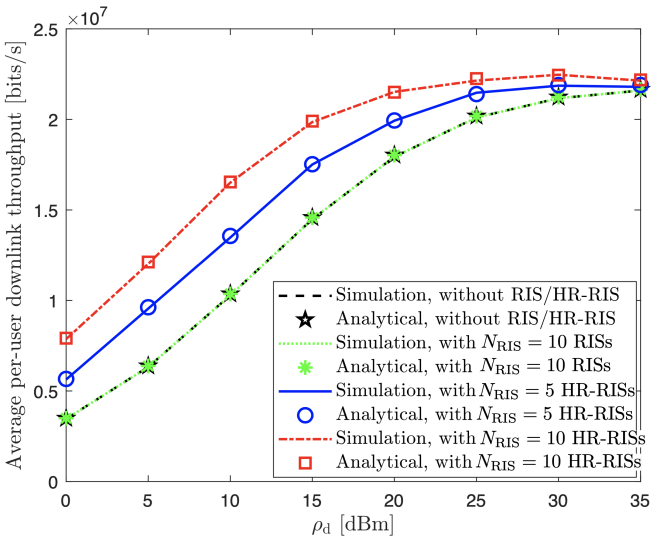

Fig. 3. Downlink per-user throughputs of passive and semi-active RIS-aided CF mMIMO systems when $N_{\rm A}=2$, $L=30$, $N_{\rm RIS}=\{5,10\}$, $M=40$, and $K=5$. Each semi-active RIS has a transmit power of -3dBm and a single active element. RIS is passive but HR-RIS is semi-active.

New interest has emerged to leverage the semi-active beamforming capability of hybrid RISs (or HR-RISs) in combining with CF mMIMO [98]. Consider a downlink communication from L APs, each with $N_{\rm A}$ antennas to K single-antenna UEs, assisted by $N_{\rm RIS}$ semi-active RISs (i.e., HR-RISs). It can be shown that the downlink per-user rate is given by [98]

$$R_k = \frac{B_0\tau_{\rm d}}{\tau_{\rm c}}\log_2\left(1+\frac{\rho N_{\rm A}^2\left(\sum_{\ell=1}^{L}\sqrt{\eta_{\ell k}}\gamma_{\ell k}\right)^2}{\rho N_{\rm A}\sum_{k'=1}^{K}\sum_{\ell=1}^{L}\eta_{\ell k}\zeta_{\ell k}\gamma_{\ell k'}+\sigma_k^2}\right), \tag{3}$$

where B_0, ρ, $\tau_{\rm d}$, and $\tau_{\rm c}$ are the system bandwidth, maximum transmit power at each AP, length of training sequence, and coherence interval, respectively. Also, $\eta_{\ell k}$ is the power control coefficient for the symbol intended for the k-th UE, and $\gamma_{\ell k}$ is the variance of the channel estimation error, which depends on the large-scale fading channel coefficients between the APs, RISs and UEs, and the reflection coefficients of the RISs.

As $LN_{\rm A}\to\infty$, the received signal in the RIS-aided system becomes free of interference and noise, like in conventional CF mMIMO systems [93]. The analytical derivation is verified in Fig. 3. It is observed that with random phase shifts, passive RISs offer negligible performance gain for CF mMIMO systems. By contrast, the semi-active RISs provide considerable throughput improvement, and the gain is more significant at low and moderate APs' transmit power. Also, it is clear that deploying more RISs offers greater improvements.

III. Surface-wave based RIS

While a conventional RIS provides a number of key benefits, using the surface as a propagation medium for surface-wave communications in addition to a reflector creates new opportunities for mobile communications. The use of surface wave is motivated by its two unique characteristics. The first is its low propagation loss compared to space wave, see (1), whereas its

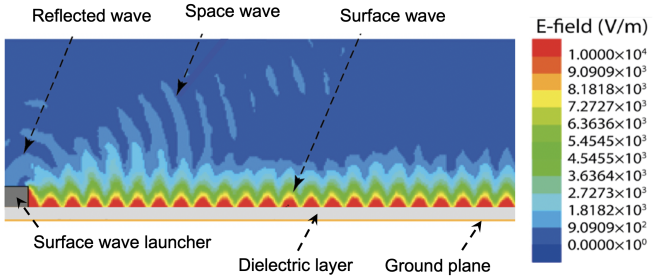

Fig. 4. A cross-section illustration of surface wave propagation at 60GHz along a surface with surface impedance of $j200\Omega$.

localized transmission leads to less interference in space while still capable of reaching the users via surfaces, see Fig. 2. It is anticipated that these new functionalities will combine with the reflection-based RIS technology to greatly enhance mobile communications in a novel way. In this section, we cover the basics of surface waves and review the required technologies that facilitate RIS to produce those phenomena.

A. Surface Waves

The discovery of radio surface waves dated back as early as 1930s by Burrows in [99]. Barlow and Cullen then provided a unified theory of various forms of surface wave and offered its physical interpretation in 1950s [57]. A comprehensive review of surface waves can be found in [100]. Of particular relevance to RIS is the non-radiating trapped surface wave propagation along an interface between two media [101], [102].

Surface wave propagates on a surface with specific surface impedance which can be realized by many inexpensive common materials such as polytetrafluoroethylene (PTFE). Fig. 4 illustrates the propagation phenomenon of surface wave for a PTFE surface. It can be seen that the radiation power mostly stays on the surface and propagates strongly along the surface. Also, the wave attenuates greatly away from the surface. The former property ensures high propagation efficiency while the latter property is desirable for interference management in the RIS application. Note that in the figure, the launcher is there to produce a radio wave on the surface and may not exist if the wave comes from elsewhere, e.g., BS. Also, the reflected wave is caused by the mismatch at the launcher which can be minimized by improving the design of the launcher.

B. Excitation Efficiency

To excite purely surface wave without space wave radiation, an ideal transducer of infinite height with exponential decay of electric field (E-field) distribution along the height would be required [57]. In reality, nonetheless, a finite-height transducer with a rectangular aperture is usually employed if the surface wave is originated from the surface [103]. In this case, space waves and/or reflected waves will exist, and it can be formally characterized by the excitation efficiency [101], [104]

$$\eta_s = \frac{P_{\rm surface}}{P_{\rm total}} = \frac{P_{\rm surface}}{P_{\rm surface}+P_{\rm space}+P_{\rm reflect}}, \tag{4}$$

where P_{surface}, P_{space} and P_{reflect} represent, respectively, the power of surface wave at the output of the launcher, the power of space wave at the output of the launcher, and that of the reflected wave at the aperture-air boundary of the launcher. Also, P_{total} is the total power at the input of the launcher.

The reflected power is caused by the impedance mismatch and can be expressed as

$$P_{\text{reflect}} = P_{\text{total}}|\Gamma_l|^2, \tag{5}$$

where Γ_l denotes the reflection coefficient at the feed port of the launcher. The total power coming out of the launcher is therefore given by $P_{\text{surface}} + P_{\text{space}} = P_{\text{total}}(1 - |\Gamma_l|^2)$. For high efficiency, the reflection coefficient of the launcher should thus be minimized by properly choosing the dimensions of the transducer's aperture. Nevertheless, for typical RIS applications, the launcher is not present and the source of the radio wave is the BS in the downlink and the UE in the uplink. In this case, the requirement on the reflection coefficient of the RIS will be different. If it is used for beamforming, the design will aim to have a large, invariant amplitude, i.e., $|\Gamma_{m,n}| \approx 1$ and a large range of controllable phase values $\angle\Gamma_{m,n}$ for each surface atom. In the case of using RIS for modulation [29], [30], independent control of both amplitude and phase of the reflection coefficient for each atom will be required.

Away from the launcher, the excitation efficiency depends mainly on the surface reactance, X_{surf}. It was found in [101] that the excitation efficiency appears to be maximum ($\sim 95\%$) if X_{surf} is around $j250\Omega$. That is to say, for RIS, the surface impedance should have its reactance close to $j250\Omega$ if surface wave is exploited to improve propagation efficiency.

C. Surface Impedance

As depicted in Fig. 4, the basic geometry of a dielectric-coated surface wave platform consists of a dielectric layer with some relative dielectric constant ε_r and thickness h, sitting on top of a metal ground plane with conductivity σ. The surface impedance of the platform is given by [57]

$$Z_{\text{surf}} = R_{\text{surf}} + jX_{\text{surf}}, \tag{6}$$

where

$$R_{\text{surf}} = \frac{1}{2}\omega\mu_0\Delta, \tag{7}$$

$$X_{\text{surf}} = \omega\mu_0\left(\frac{\varepsilon_r - 1}{\varepsilon_r}h + \frac{\Delta}{2}\right), \tag{8}$$

where ω denotes the operating angular frequency, $\mu_0 = 4\pi \times 10^{-7}\text{Hm}^{-1}$ is the permeability of free space, and $\Delta = \sqrt{\frac{2}{\omega\mu_0\sigma}}$ is the skin depth of a copper sheet. Also, we can define the relative permittivity of the surface platform by

$$\varepsilon_{\text{surf}} \triangleq \frac{Z_0^2}{Z_{\text{surf}}^2}, \tag{9}$$

where $Z_0 \approx 377\Omega$ is the intrinsic impedance of free space.

The surface impedance of the platform can be reconfigured via the meta-atoms if they are connected to electronic devices such as varactor diodes. Fig. 5 shows an architecture that can tune the effective impedance of each meta-atom, Z_{atom}, using

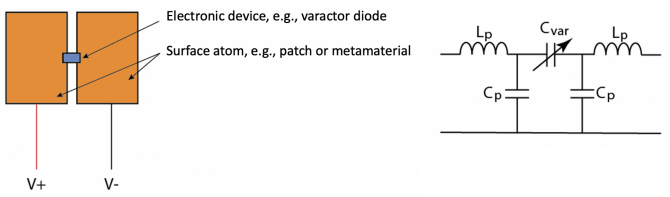

Fig. 5. The geometry of a possible reconfigurable surface meta-atom and its simplified equivalent circuit model assuming a varactor diode connection.

a varactor diode. In the model, C_{var} is the variable capacitance controllable by the biasing voltage of the varactor diode, and L_p and C_p denote, respectively, the intrinsic inductance and capacitance of the rectangular pads. By altering C_{var}, we can obtain a prescribed effective capacitance of each meta-atom, C_{eff}, which in turn influences the meta-atom impedance by

$$Z_{\text{atom}} = Z_0\sqrt{\frac{C_0}{C_{\text{eff}}}}, \tag{10}$$

where C_0 denotes the capacitance of air substrate and C_{eff} is geometry specific and depends on L_p, C_p and C_{var}. There is a relationship between the meta-atom impedance and the effective surface impedance of the reconfigured surface, which will be given in (19) later in Section III-F.

Having the ability to reconfigure the effective impedance for each meta-atom (by, e.g., varactor diode) is important as it empowers the surface to change its characteristics at liberty. In Section III-F, transition from surface wave to space wave using reconfigurable meta-atoms will be discussed.

D. Path Loss

Given a plane wave propagating on a surface, the E-field of the surface wave in the cylindrical coordinate system with z being the vertical distance from the surface and r the radial propagation distance, can be expressed as [105][6]

$$E_r = A\left(\frac{u_2}{j\omega\varepsilon_0}\right)e^{-u_2 z}H^{(2)}(-j\gamma r), \tag{11}$$

where A is a scaling constant, $H^{(2)}$ is the Hankel function of the second kind,

$$u_2 \approx \frac{\omega^2\mu_0\varepsilon_0}{\sqrt{2\omega\mu_0\sigma}} \times \left[\left(1 - \frac{\omega\varepsilon_0(\varepsilon_r + 1)}{2\sigma}\right) + j\left(1 + \frac{\omega\varepsilon_0(\varepsilon_r + 1)}{2\sigma}\right)\right], \tag{12}$$

$\varepsilon_0 = 8.854 \times 10^{-12}\text{Fm}^{-1}$ is the permittivity of free space, and γ is the propagation constant along the surface, given by

$$\gamma = \gamma_\alpha + j\gamma_\beta = \gamma_\alpha^{\text{d}} + \gamma_\alpha^{\text{c}} + j\gamma_\beta. \tag{13}$$

The parameters γ_α^{d} and γ_α^{c} account for the losses due to the surface material. If the dielectric surface does not involve any conducting structures, then the conduction loss will be zero

[6]To study the propagation loss of a surface wave, the literature considered a point source emitting a wave on a surface, and therefore the cylindrical coordinate system was used to help conduct the analysis.

and $\gamma_\alpha^{\mathrm{c}} = 0$. On the other hand, $\gamma_\alpha^{\mathrm{d}}$ is related to the loss tangent $(\tan\delta)$, given by

$$\gamma_\alpha^{\mathrm{d}} = \frac{\omega\sqrt{\varepsilon_r}}{2c}\tan\delta, \tag{14}$$

which is sufficiently small to be ignored for typical substrates. For PTFE as an example, $\tan\delta$ is in the order of 10^{-3} at 10GHz. In what follows, $\gamma \approx j\gamma_\beta$. Under this setup, for large r, the Hankel function can be approximated by

$$H^{(2)}(-j\gamma r) \approx \sqrt{\frac{2}{\pi\gamma_\beta r}}e^{-j\left(\gamma_\beta r+\frac{3\pi}{4}\right)}. \tag{15}$$

Combining (11) and (15) and replacing r by d to denote the propagation distance, we have

$$E_r \propto \frac{1}{\sqrt{d}}. \tag{16}$$

In other words, the received power of surface wave over distance satisfies $P_{\mathrm{SW}} \propto d^{-1}$. This is the classical path loss result for surface wave propagation. As a matter of fact, the path loss exponent can be further improved using reconfigurable structures on the surface which will be discussed later.

E. Non-Flat and Broken Surfaces

Surface wave has robust connectivity and the surface does not need to be perfectly flat to support the transmission. Fig. 6 shows the case of a curved surface in which the surface wave makes a smooth 90° turn round the corner. The results reveal that the surface wave still possesses large radiated power after the curved turn. The noticeable space waves are caused by the sharp edge discontinuities for a relatively narrow surface. In addition, the space and reflected waves around the transducers can be ignored as the transducers are there only to generate the surface wave but in the RIS application, the source of the radio waves is external from the BS or UEs. Fig. 7(a) further demonstrates that surface wave propagation is sustained even if the surface makes angled turns although the discontinuities at the turns do emit more space waves. In the RIS application, where the UEs are away from the surface, however, angled surfaces could be exploited, if suitable, to produce the needed space waves to reach the UEs away from the surface.

Furthermore, surface wave is surprisingly robust to gaps on the surface due to damage, knowing the fact that an RIS may be installed in an outdoor environment. Fig. 7(b) looks at this situation and examines the impacts on the surface wave propagation. It can be observed that while the gap introduces discontinuities, the wave is able to leap across the gap and continue to glide along the surface after the gap. Evidently, the gap causes space waves to emit and typically the larger the gap the more the space wave as a consequence.

F. Switching between Surface and Space Waves

RISs deployed in the environment are aimed to bridge the communication between BS and UEs. If the RIS operates as a reflector, then the working principle is relatively straightforward and the radio signals naturally come off the surface via the reflection coefficients of the surface atoms to reach

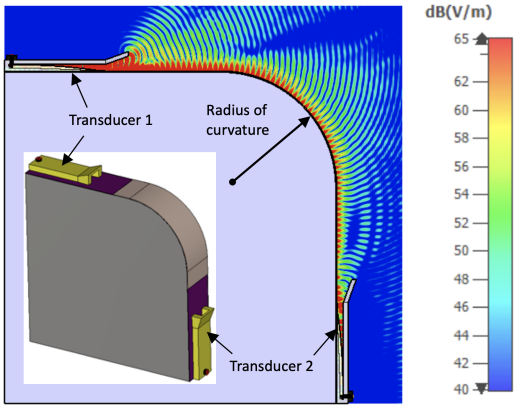

Fig. 6. Surface wave propagation over a curved surface with 10 free-space wavelengths of the operating frequency as the radius of curvature at the turn.

the UEs after propagating onto the surface from the BS. The challenge is to acquire the CSI and optimize all the reflection coefficients at once to shape the reflected beams [106], [107]. By contrast, the RIS utilizing surface waves does require a transition from surface wave to space wave. Such transition can be realized by introducing discontinuities on the surface.

To do so, one approach is to create a change in the surface impedance from one section of the surface to another. The discontinuity introduced by the change in surface impedance will lead to space waves off the surface. The surface impedance can also be optimized to launch space wave from the surface. In [108], [109], it is found that the required surface impedance of a meta-surface to launch a space wave at an angle θ^* (measured from the normal of the surface) is given by[7]

$$Z_{\text{meta-surface}} = -\frac{jZ_0}{\cos\theta^*}\cot\frac{\Phi_r}{2}, \tag{17}$$

where

$$\Phi_r(d,\omega) = \frac{\omega d(\sin\theta^* - \sin\theta_{\text{in}})}{c} + \Phi_0(\omega), \tag{18}$$

where d represents the propagation distance which also marks the position on the surface, θ_{in} denotes the incident angle of the wave, c is the speed of light, and $\Phi_0(\omega)$ denotes the initial phase of the surface wave at $d = 0$. The corresponding effective impedance of the meta-atom for achieving the required $Z_{\text{meta-surface}}$ can also be found as

$$Z_{\text{atom}} = \frac{jZ_{\text{meta-surface}}Z_{\text{surf}}\tan(\beta_{\text{surf}}h)}{jZ_{\text{surf}}\tan(\beta_{\text{surf}}h) - Z_{\text{meta-surface}}}, \tag{19}$$

in which $\beta_{\text{surf}} = \omega\sqrt{\mu_0\varepsilon_0\varepsilon_{\text{surf}}}$ and Z_{surf} and $\varepsilon_{\text{surf}}$ have been defined in (6) and (9), respectively. As a result, given the requirement (17), we can find the needed Z_{atom} by (19) and achieve this using the method discussed in Section III-C.

Another approach is to use preinstalled metallic structures on the surface. The metallic structures provide the discontinuities on the surface that diffract the surface wave to the space and the pattern of the structure can be designed accordingly to

[7]Note that Z_{surf} refers to the surface impedance of the platform without the reconfigurability while $Z_{\text{meta-surface}}$ concerns the effective surface impedance with reconfigurable meta-atoms.

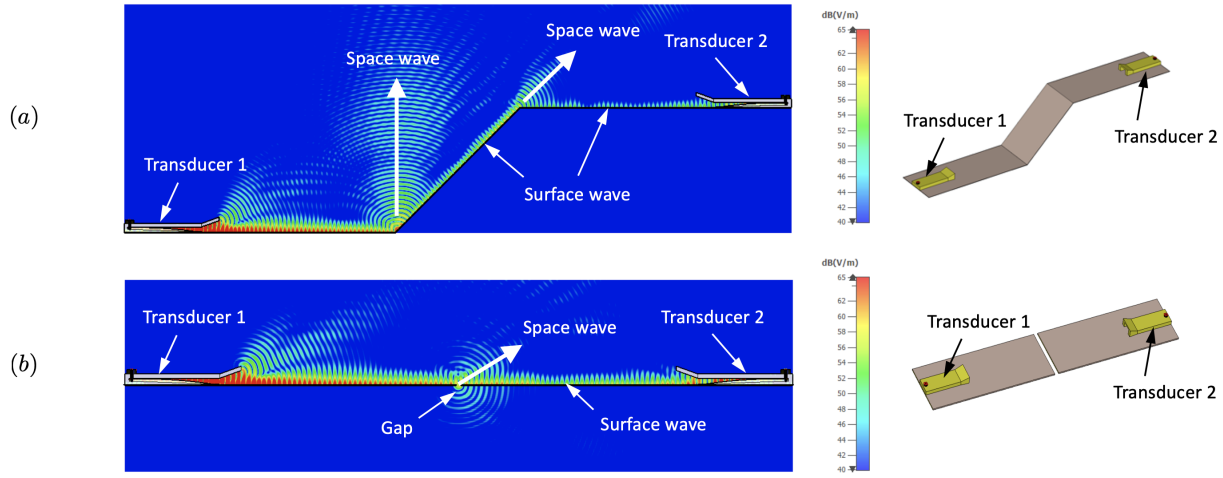

Fig. 7. Surface wave propagation over a surface with (a) 45° cornered turns and (b) a gap of 0.4 wavelengths.

steer the space wave towards a given direction. The transition from surface wave to space wave using diffraction patterns can be explained by leaky-wave and holographic antenna theories [110]–[113]. When a surface wave is incident onto metal patterns, the dimensions of the patterns will determine the leakage rate of the wave, and the leaky wave will be excited with the proper mode phase velocity and the degree of coupling to the metal patterns [113]. The works in [114], [115] have provided the analysis for the relationship between the launching angles with different pattern parameters. Fig. 8 provides the three-dimensional EM simulation results of some simple periodic metallic structures on a surface, illustrating the wave transition. The results illustrate that surface wave can be diffracted to produce space wave at a launching angle from the platform through periodic metal square patten geometries. The direction of the space wave varies with the size of the metallic squares and the spacing between them.

G. Reconfigurable Surface Platform

Reconfigurable meta-atoms have been discussed in Sections III-C & III-F, which equips the surface the ability to adapt the surface wave and space wave for transmission. In fact, more can be done on the surface to enhance the reconfigurability of the platform. Despite the superior path loss when compared to space wave propagation (see Section III-D), the path loss of surface wave propagation can be improved further if reconfigurable conductive structures are adopted on the surface. In [59], a reconfigurable surface platform where small tubes of controllable feed of conductive fluid are installed, is proposed. Fig. 9(a) illustrates the setup where the conductive fluid can come from underneath the surface when needed via digitally controlled nano-pumps. In practice, the tubes should be spread all over the entire surface so that high-resolution control of the surface wave on the entire surface can be achieved. A more thorough, practical design using a punctured surface platform is given in [116]. The punctured cavities allow conductive fluid to appear on demand to control the surface waves.

The advantages of the use of conductive bars are twofold. First, it can be used to create a pathway resembling a waveguide for concentrating the power of the surface wave, as is the purpose of the setup in Fig. 9(a) where two rows of bars filled with Galinstan are installed. In so doing, the pathway has an effect similar to beamforming so that the path loss of surface wave can be considerably reduced. In Fig. 9(b), the results for the received power of the surface wave over the distance along the pathway are provided. The corresponding results without the Galinstan bars are also given for comparison. As we can see, the attenuation of the received power over distance in the case with the bars is negligible (i.e., the path loss exponent $\alpha \approx 0$) while the same cannot be said without the Galinstan bars. It is also possible to concentrate the surface wave power even more if more layers of Galinstan bars are employed but rigorous analysis will be required in the future.

Another advantage is that turned pathways can be formed to cater a variety of communication needs. Making sharp turns for surface wave is not challenging. What it takes is simply to feed the bars at the required locations with conductive fluid, e.g., Galinstan in this example. The results in Fig. 10 illustrate such possibilities and it can be observed that the surface wave can make 90° turns and also support multi-way transmissions. Besides, in all the cases considered, the power of the surface wave remains very strong within the pathways. It is noted that surface waves making sharp turns were also independently studied in [117] but the work required mechanically controlled metal bars, which is practically difficult to achieve.

IV. Fluid Antenna System

In this section, we switch our attention to another emerging technology, a new antenna technology that can combine with MIMO and RIS in mobile communications. Conventional antennas are usually made of solid materials, such as metal wires, plates, dielectric slabs and etc. Their predefined geometries limit their performances in dynamic wireless environments. In contrast, an antenna made of fluid has no predefined form and can be shaped to any desirable form and mobilized to adapt to the ever-changing wireless environments. This idea may be realized using reconfigurable pixels [41], [42]. Such antenna can be broadly referred to as 'fluid' antenna. Here, we review

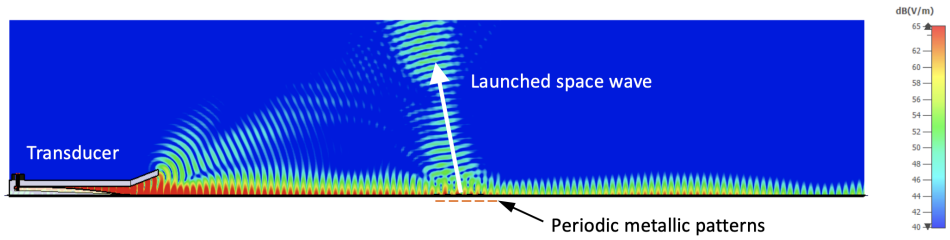

Fig. 8. Launching of space waves from the surface, pointing direction of -15° by a 5×15 2mm-square periodic metallic pattern.

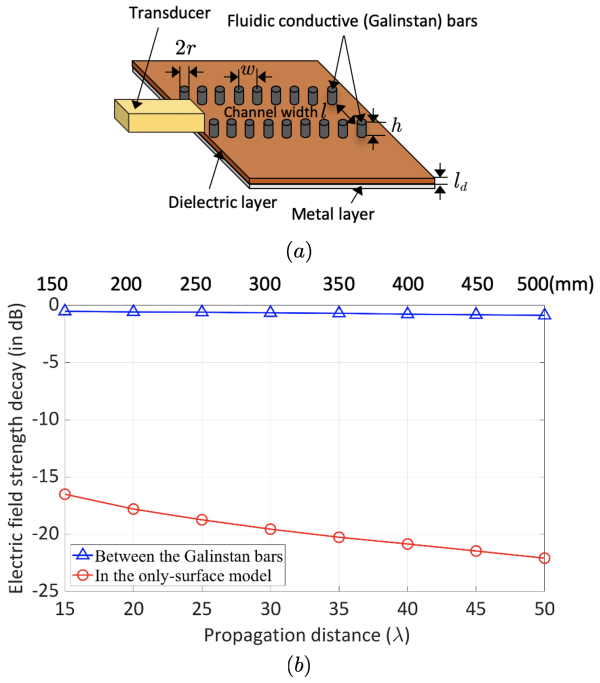

Fig. 9. (a) A reconfigurable surface platform using fluidic conductive bars; (b) the received power of surface waves against the propagation distance.

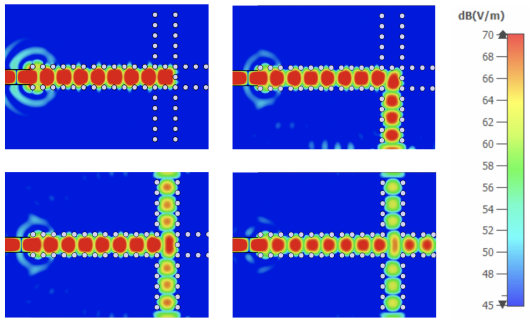

Fig. 10. Pathways created by Galinstan bars to facilitate turned transmissions.

the basic architecture of some well-known fluid antennas and cover the theoretical result that can be useful in the context of the design of mobile communications networks.

A. Basic Structure

Reconfigurable antennas have been one of the hot research topics for decades [118], [119] but the research for fluid antennas is only heating up over the last ten years, mainly because

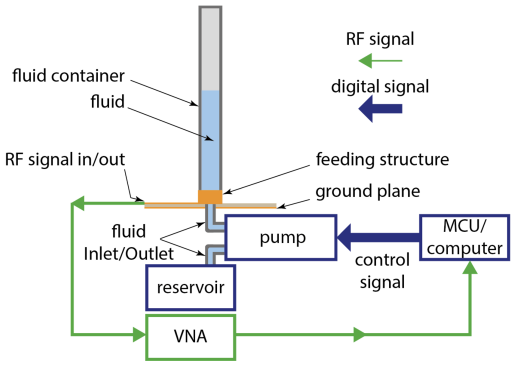

Fig. 11. The monopole fluid antenna.

of the concern in radiation efficiency compared to conventional solid-based antennas. Recent high-profile successes such as the highly efficient seawater antenna system by Mitsubishi Electric [51] and the beam-steering network using seawater antennas in [52], [53] have helped fluid antenna research gather pace. So far, there have already been a rich literature of fluid-type antennas that focus on a range of reconfigurability [50]. Here, we describe two most relevant types of fluid antenna.

1) Monopole Fluid Antenna: The first type is a frequency-agile monopole fluid antenna system [44]. Fig. 11 illustrates the basic architecture of the frequency-agile fluid monopole antenna system where the resonant frequency can be adjusted. Variants can be derived based on the required reconfigurabilities and applications. However, the key components are (1) the feeding network for delivering/collecting the RF signal, (2) the fluid serving as the sole or part of the radiating element, (3) the fluid container and reservoir for holding the fluid, and (4) the pump, feedback mechanism and the corresponding control unit for changing the antenna performance.

The feeding network is responsible for delivering or receiving the RF signal to or from the radiating element. In the case of frequency diversity, wideband feeding geometries are required. Also, independent performance tuning and leakage-free environment are important. Direct-contact feeding methods are sensitive to the change of fluid volume in the container which will incur impedance matching problems [120]. Hence, coupling-fed methods which indirectly deliver/collect the RF signal from the radiating element are preferred [121], [122].

The fluid, depending on their electrical properties, can be considered either metallic, e.g., mercury and Eutectic Gallium-Indium (EGaIn), or dielectric, such as, pure water and ionized

solution, radiating element [123]. Liquid metal radiating element can be EM-modelled like common metals with specific conductivity, whereas fluid antennas using water or ionized solution can be categorized as a dielectric resonator antenna (DRA), with the resonant frequencies determined by its size, shape, material and permittivity [124], [125].

The fluid should be kept in a container when in use or in the reservoir as reserve. Currently, there are two main processes to assemble the container. One material used is PDMS (polydimethylsiloxane). This is a flexible and deformable elastomer that is commercially available. Photolithography is first used to create the microchannels in the PDMS container and then let the fluid flow in to create the radiating elements [47]. Another option is to use a 3D printer to fabricate the container using resin. Several designs using 3D printing for rapid prototyping of fluid antennas were presented in [44], [126], [127].

The pump is employed for flowing the fluid in and out of the container for tuning the antenna performance. Micro-pumps [128] or nano-pumps [129] are required. The microcontroller unit (MCU)/computer is there to control the fluid flow. In the case of frequency diversity, a vector network analyzer (VNA) is used to measure the reflection coefficient of the antenna.

2) Surface Wave Based Fluid Antenna: Though frequency-agile antennas are useful in cognitive radio applications [130], [131], fluid antennas can certainly do more. Another type of fluid antenna concerns with the ability to adjust the position and/or the radiation pattern of the antenna [132]. Having this ability enables the antenna to exploit the ups and downs of wireless channels resulting from distinctive superposition of multipath due to scattering in the environments. The benefits can be formally characterized using communication theory and will be summarized in Sections IV-C and IV-D later.

The technology that produces a position-flexible antenna is surface wave based fluid antenna [132]. As discussed above in Section III, when a surface wave propagating along a dielectric medium is diffracted by metallic geometries, current will be induced and the surface wave will be scattered into the free space, creating a radiation pattern. This same principle can be applied to design a position-flexible antenna. Fig. 12 depicts the geometry of the surface wave based fluid antenna where the fluid radiator scatters the E-field onto free space for radiation and the position of the fluid radiator is tuneable by the micro-pumps. Fig. 13 further shows the E-field distributions of the geometry with and without the fluid radiator. As we can see from the results, the fluid radiator with $L_{\text{fluid\_start}} = 25\text{mm}$ can produce a directional radiation pattern (pointing to 65°). Note that this is achieved with a single RF chain. Presumably, the direction of the radiation pattern would be changeable by optimizing the position and shape of the fluid radiator but more work will need to be carried out in this area.

3) Others: Apart from the above designs acting as the main radiating element of the antennas, fluid has also been used as parasitic elements, loading elements or switches. A center-feed parasitic circular patch antenna with continuously tuning linear polarization capability was reported in [133]. Based on the Yagi-Uda antenna concept, distilled water was loaded or unloaded as the reflector or director for changing the radiation pattern in [134], whereas a 360° beam steering was obtained

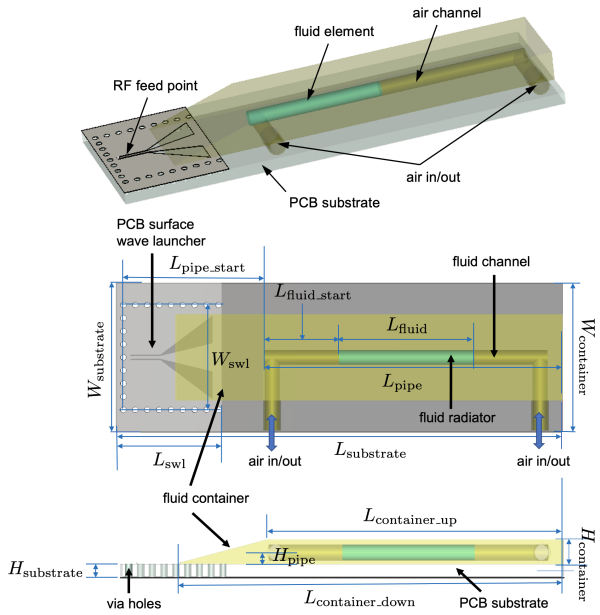

Fig. 12. The surface wave based fluid antenna.

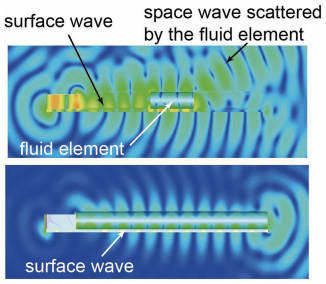

Fig. 13. The E-field distributions with and without the fluid radiator.

in the salty water antenna described in [53].

In liquid-based fluid antennas, response time is a legitimate concern as mobilizing fluid from one point to another takes time, however small. To overcome the response time limitation, another option is to use reconfigurable pixels to emulate the agility of fluid by turning on and off pixels intelligently to form changeable radiating structures [41], [42].

B. Type of Fluids and Their Characteristics

The choice of fluid radiator deserves careful consideration. Liquid metal and metal alloy have high conductivity, ranging from $1 \times 10^6 \text{Sm}^{-1}$ to $3.46 \times 10^6 \text{Sm}^{-1}$ at 20°C, when it is used in antenna design, and the radiation efficiency is higher than that of dielectric solution. Nonetheless, mercury is toxic, and its high surface energy tends to minimize surface area which prevents it from forming mechanically stable structures. Although Galinstan and EGaln [135] are usually used in fluid antenna designs, they are highly corrosive against other solid metals commonly used in electronic circuits [136].

Alternatively, water and ionized solution are low-cost, eco-friendly and easily accessible, but its high freezing point, evaporation, and low conductivity are the challenges. Researchers have attempted to use anti-freezer to lower the freezing point

of water [137], but the antenna suffers from its high temperature sensitivity resulting in large frequency fluctuation [50]. Solvent-based, oil-based fluid and ionized solution have also recently been used for realizing fluid antennas. The solvent-based fluid antennas utilizing ethyl acetate with polarization diversity have demonstrated over 80% of radiation efficiency in the frequency range of 3.5 to 4.5GHz [138], [139], but the materials for building the container must be carefully chosen to avoid potential chemical reaction and damage. Oil-based fluid antennas with good frequency tuning range and high efficiency have also been reported in [140], [141]. The antennas are more chemically stable but at the price of a larger antenna size. In addition, the viscosity of the oil-based fluid will affect the flow speed, giving rise to a longer response time.

C. Diversity Gain

Given the recent advances in fluid antennas, it is anticipated that position-flexible antennas will become reality for years to come. The early results for surface wave based fluid antennas suggest that the position of the fluid radiator can be tuned with nearly infinite resolution if we have sufficiently high resolution control of the pump. The implication can be massive. In [38], [39], Wong *et al.* studied a wireless communication system in which a position-flexible fluid antenna is used at the receiver. Specifically, the fluid radiator is assumed to always move to the best of N predefined positions (referred to as 'ports') for minimal outage probability performance. In the following, we summarize some key results that give important insight.

Note that a UE typically only has a small space to house the antenna, the fluid radiator is not expected to have a large space for exploitation. Additionally, if high-resolution control of the radiator's position is possible, i.e., large N, the wireless channels seen by the fluid radiator at nearby ports will be very highly correlated. Assuming rich scattering (Rayleigh fading envelope) and modelling the fluid radiator at a given port as an ideal omnidirectional point antenna, the outage probability of a fluid antenna system can be defined based on an outage event with an average SNR target, $\bar{\gamma}$, i.e.,

$$\mathcal{O}_{\mathrm{SNR}}(\gamma_{\mathrm{th}}) = \left\{ \max_k |g_k|^2 < \frac{\bar{\gamma}}{\Theta} \equiv \gamma_{\mathrm{th}} \right\}, \tag{20}$$

in which g_k denotes the channel at the k-th port of the fluid antenna, Θ represents the average symbol energy to the noise power and γ_{th} denotes the normalized SNR target. In [39], it was reported that the outage probability of the fluid antenna system is given by

$$\mathrm{Prob}\left(\mathcal{O}_{\mathrm{SNR}}(\gamma_{\mathrm{th}})\right) = \int_0^{\frac{\gamma_{\mathrm{th}}}{\Gamma}} e^{-t} \times \prod_{k=2}^{N} \left[1 - Q_1\left(\sqrt{\frac{2\mu_k^2}{1-\mu_k^2}}\sqrt{t}, \sqrt{\frac{2}{1-\mu_k^2}}\sqrt{\frac{\gamma_{\mathrm{th}}}{\Gamma}} \right) \right] dt, \tag{21}$$

where $\Gamma = \sigma^2\Theta$ is the average received SNR at each port, σ^2 is the average power of the channel seen at each port, $Q_1(a,b)$ denotes the first-order Marcum Q-function, and

$$\mu_k = J_0\left(\frac{2\pi(k-1)}{N-1}W\right), \text{ for } k = 2, \ldots, N,^{8} \tag{22}$$

where $J_0(\cdot)$ is the zero-order Bessel function of the first kind and the space for the fluid radiator to move is $D = W\lambda$ with λ being the wavelength of radiation. Fig. 14 shows the geometry of such fluid antenna system with N fixed ports.

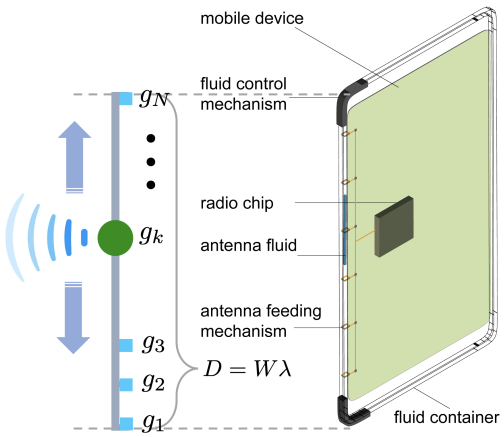

Fig. 14. The geometry of a fluid antenna system with N ports where $\{g_k\}$ are the complex channel envelopes at the ports. For single-user systems, the best port is defined as $\max\{|g_k|\}$ to obtain the maximum received SNR.

To gain more insight, an upper bound can be obtained as

$$\mathrm{Prob}\left(\mathcal{O}_{\mathrm{SNR}}(\gamma_{\mathrm{th}})\right) < \left(1 - e^{-\frac{\gamma_{\mathrm{th}}}{\Gamma}}\right) \prod_{k=2}^{N} \left(1 - \frac{\varrho}{\sqrt{|\mu_k|}} e^{-\frac{\kappa}{1-\mu_k^2}\left(\frac{\gamma_{\mathrm{th}}}{\Gamma}\right)} \right), \tag{23}$$

where $\kappa > 1$ can be any constant and

$$\varrho \triangleq \frac{e^{\frac{1}{\pi(\kappa-1)+2}}}{2\kappa} \sqrt{\frac{(\kappa-1)(\pi(\kappa-1)+2)}{\pi}}. \tag{24}$$

From this upper bound, it can be seen that the k-th antenna port contributes to a diversity gain of $\frac{\varrho}{\sqrt{|\mu_k|}}$ but comes with an SNR scaling penalty of $\frac{1-\mu_k^2}{\kappa}$, see [39, Corollary 4]. More remarkably, it can be shown that the fluid antenna system with some finite dimension $W > 0$ can achieve any arbitrarily small outage probability, if $N \to \infty$ [39, Theorem 8]. This reveals that the diversity can be enormous even with a small space.

Also, the outage performance of the fluid antenna system (with a single RF chain) can outperform that of an L-branch maximal ratio combining (MRC) system (with L RF chains and independent branches) if the number of ports satisfies

$$N > 2 \left\lceil \frac{\ln\left(\frac{p_{\mathrm{out}}^{\mathrm{MRC},L}(\gamma_{\mathrm{th}})}{1-e^{-\frac{\gamma_{\mathrm{th}}}{\Gamma}}}\right)}{\ln\left(1 - \frac{\varrho}{\sqrt{|J_0(\pi W)|}} e^{-\frac{\kappa}{1-J_0^2(\pi W)}\left(\frac{\gamma_{\mathrm{th}}}{\Gamma}\right)}\right)} + 1 \right\rceil, \tag{25}$$

where

$$p_{\mathrm{out}}^{\mathrm{MRC},L}(\gamma_{\mathrm{th}}) = 1 - e^{-\frac{\gamma_{\mathrm{th}}}{\Gamma}} \sum_{k=0}^{L-1} \frac{1}{k!} \left(\frac{\gamma_{\mathrm{th}}}{\Gamma}\right)^k \tag{26}$$

[8] Recently in [142], it was proposed to set all the $\{\mu_k\}$ to be equal so that the correlation between any two ports can be better modelled.

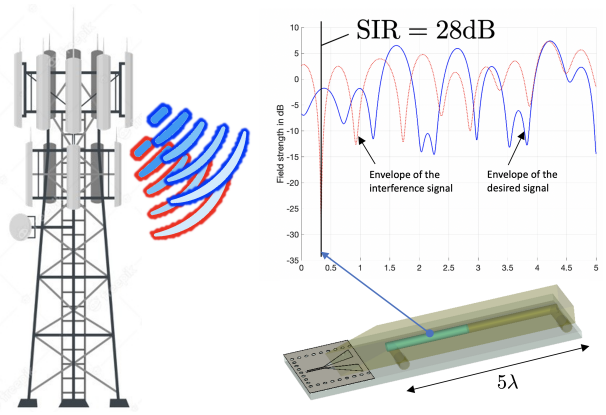

Fig. 15. Multiple access by exploiting the deep fade of interference.

is the outage probability for the L-antenna MRC system. Note that (25) is observed by combining the results in Corollary 6 and Theorem 9 of [39]. While the superiority of fluid antenna may be counter-intuitive, it comes directly from the ability to change the position of the fluid radiator at high resolution, i.e., large N, to exploit the differences in the fading envelopes.

The diversity gain of fluid antenna can also be translated into capacity gain and such results were reported in [38].

D. Multiple Access and Multiplexing Gain

The main advantage of fluid antenna lies in its ability to deal with multiuser communications [143]. Fluid antenna allows a UE to observe the fading envelopes in the available space and switch the fluid radiator to the position where the interference suffers from a deep fade to facilitate multiple access. Fig. 15 shows the concept of using fluid antenna for multiple access (FAMA). For this to work, it requires that the desired signal and the interference signal have independent fading envelopes at the UE. This is naturally achieved if the multiuser signals come from different BSs (e.g., in multicell environments or device-to-device applications). In the downlink, it is possible if multiple antennas are present at the BS and multiuser signals are made independent by random beamforming or each user's signal is transmitted from a dedicated BS antenna.

There are two approaches to achieve FAMA. The first one is referred to as fast FAMA (i.e., f-FAMA) in which the fluid antenna is expected to switch to the best port and track the interference null on a symbol-by-symbol basis. In this case, the outage event can be defined based on a target symbol-level signal-to-interference ratio (SIR) threshold, γ, i.e.,

$$\mathcal{O}_{\text{SIR}}^{f\text{-FAMA}}(\gamma) = \left\{ \max_k \left| \frac{g_k s}{\sum_{\ell=1}^{N_\text{I}} g_k^{(\ell)} s_\ell} \right|^2 < \gamma \right\}, \tag{27}$$

where s_ℓ denotes the information symbol from the ℓ-th interferer and $g_k^{(\ell)}$ is the channel from this interferer encountered at the k-th port of the user of interest. Assuming $|s| = 1$ for simplicity, the outage probability for f-FAMA has been provided in [143, Theorem 1], which is given as (28) (see top of next page), where $I_0(\cdot)$ represents the zero-order modified Bessel function of the first kind, σ_I^2 is the average power of the accumulated interference, $\sigma^2 = \text{E}[|g_k|^2] = \text{E}[|g_k^{(\ell)}|^2]$, and μ_k has been defined before in (22). Notice that the interference immunity is not decided by the number of interference signals but their sum average power. A larger number of interference signals actually causes deeper fades. The achievable multiplexing gain, m, of the f-FAMA network is given by

$$m = (N_\text{I}+1)\left(1 - \text{Prob}\left(\mathcal{O}_{\text{SIR}}^{f\text{-FAMA}}(\gamma)\right)\right), \tag{29}$$

which is lower-bounded by [143, Corollary 4]

$$\begin{aligned} m &\overset{(a)}{\gtrsim} \min\left\{ \frac{\left(\lfloor \frac{N}{2} \rfloor - 1\right)\left(1 - J_0^2(\pi W)\right)(N_\text{I}+1)}{\left(\frac{\sigma_\text{I}^2 \gamma}{\sigma^2}\right)}, N_\text{I}+1 \right\} \\ &\overset{(b)}{\approx} \min\left\{ \frac{\left(\lfloor \frac{N}{2} \rfloor - 1\right)\left(1 - J_0^2(\pi W)\right)}{\gamma}, N_\text{I}+1 \right\}, \end{aligned} \tag{30}$$

where N_I denotes the number of interferers (or $N_\text{I}+1$ is the total number of UEs), and (b) uses the fact that $\sigma_\text{I}^2 = N_\text{I}\sigma^2$. The multiplexing gain, m, measures the number of times the network capacity compared to a single-user capacity.

Corollary 1 in [143] reveals that given all other parameters fixed, as $N \to \infty$, $\text{Prob}\left(\mathcal{O}_{\text{SIR}}^{f\text{-FAMA}}(\gamma)\right) \to 0$, which means that if the fluid antenna has infinite resolution, the interference can always be resolved. Theorem 8 in [143] gives an estimate on how large N needs to be for a given performance.

While fast port selection to track and tune in to the interference null performs very well, it can be problematic in terms of complexity and response time. Alternatively, the fluid antenna can be operated to change its port on a block-by-block basis only. In other words, a port once selected remains activated until the channels change to demand a re-optimization. In this case, FAMA attempts to find a region (or ports) where all the fading envelopes of the interferers dip and that of the desired signal is acceptable so that the reception quality remains good independent of the information symbols from the interferers. This is referred to as slow FAMA (i.e., s-FAMA) which has the outage event defined based on the average SIR as

$$\mathcal{O}_{\text{SIR}}^{s\text{-FAMA}}(\gamma) = \left\{ \max_k \frac{|g_k|^2}{\sum_{\ell=1}^{N_\text{I}} \left|g_k^{(\ell)}\right|^2} < \gamma \right\}, \tag{31}$$

where it has been assumed that $\text{E}[|s|^2] = \text{E}[|s_\ell|^2]$. Presumably, similar analysis to [143] can be obtained.

E. Port Selection

The performance of fluid antenna systems relies on the fact that the 'best' port is known. This is a straightforward task if all the ports are observed. However, for large N, this becomes infeasible due to excessive channel estimation and response time. A more realistic scenario is when only a few ports are observed to reason and deduce the best port by exploiting the spatial correlation among the ports. In [144], this problem was addressed for single-user fluid antenna systems using learning-based methods. How these methods fare for FAMA is however not understood and should be properly investigated.

$$\text{Prob}\left(\mathcal{O}_{\text{SIR}}^{f\text{-FAMA}}(\gamma)\right) = \int_0^{\infty} e^{-z} \int_0^{\frac{\sigma_{\text{I}}^2\gamma}{\sigma^2}z} e^{-t} \left\{ \prod_{k=2}^{N} \left[1 + \left(\frac{\frac{\sigma_{\text{I}}^2\gamma}{\sigma^2}}{\frac{\sigma_{\text{I}}^2\gamma}{\sigma^2}+1} \right) e^{-\left(\frac{1}{\frac{\sigma_{\text{I}}^2\gamma}{\sigma^2}+1}\right)\frac{\mu_k^2}{1-\mu_k^2}\left(\frac{\sigma_{\text{I}}^2\gamma}{\sigma^2}z+t\right)} \times I_0\left(\frac{\frac{\sigma_1\sqrt{\gamma}}{\sigma}}{\frac{\sigma_{\text{I}}^2\gamma}{\sigma^2}+1} \left(\frac{2\mu_k^2}{1-\mu_k^2}\right)\sqrt{zt} \right) - Q_1\left(\frac{1}{\sqrt{\frac{\sigma_{\text{I}}^2\gamma}{\sigma^2}+1}} \sqrt{\frac{2\mu_k^2}{1-\mu_k^2}}\sqrt{t}, \sqrt{\frac{\frac{\sigma_{\text{I}}^2\gamma}{\sigma^2}}{\frac{\sigma_{\text{I}}^2\gamma}{\sigma^2}+1}} \sqrt{\frac{2\mu_k^2}{1-\mu_k^2}}\sqrt{z} \right) \right] \right\} dtdz, \quad (28)$$

V. Wireless Communications with RIS and Fluid Antennas

MIMO has been the capacity driver for mobile communications for decades and will continue to be so beyond 5G. The main issue is however the over-reliance of BS densification in order for MIMO to be effective when moving up the operating frequency. The introduction of RIS alleviates this problem by making available large apertures (via many unit cells spread over large surfaces) to help collect radio waves and redirect them to the UEs, extending the coverage area of the BS.

Nonetheless, conventional RIS has its own limitations. First, current meta-atom technology relies on a patch design which has a relatively small bandwidth in which the amplitude of the reflection coefficient is not severely attenuated and that the phase of the reflection coefficient has a good dynamic range. Second, the full range of phase control for each meta-atom is still less than 2π, not to mention the fact that the amplitude cannot be independently controlled. Furthermore, in the case of multi-carrier communications (e.g., orthogonal frequency-division multiple-access (OFDM)), the reflection coefficients of each meta-atom over different subcarriers are coupled and cannot be independently changed. Besides, RIS comes with a very large number of meta-atoms, meaning that beamforming from RIS to UEs will require complex optimization and that a large number of CSI be estimated and available at the RIS. Note that while RIS intends to be an intelligent reflector, it is not expected to have the computing power for those complex optimization and managing the CSI estimation process.

With a view to overcome the above-mentioned challenges, this section discusses what surface-wave aided RIS and fluid antenna may offer. Fig. 16 indicates how MIMO, RIS and fluid antennas combine together to provide communications from a BS to UEs via a RIS. In this example, the direct path between the MIMO BS and the UEs is severely blocked and the RIS provides a strong reflected path to reach the UEs. In particular,

- MIMO at the BS provides a focused signal beam carrying high-speed multiuser data towards the RIS, avoiding the obstacles in between the BS and the UEs.
- The RIS can act as a reflector to reach the UEs. Instead of complex optimization of the reflection coefficients of the meta-atoms or unit cells, random selection of the reflection coefficients can be used so that the RIS behaves like a large number of scatterers to cause sufficient signal envelope fluctuations at fluid antennas of the UEs and greatly liberate the bandwidth of the RIS. FAMA is then applied at the UEs for multiple access.
- The RIS can also take the incident radio waves and let them glide along the surface before hopping off to reach the intended UE. By doing so, radio waves are inherently bound to the surface until they are routed to a location close to the UE. Hence, the signals arriving at the target UE would be strong and the potential interference in the space could also be minimized. In addition, RIS is best suited to capture the tangential signals coming onto the surface and turn them into useful signals at the UEs.

In the following, we elaborate on the techniques of RIS and fluid antennas and how they shine in mobile communications.

A. Randomized RIS and FAMA

Multiple access in the downlink via RIS is more challenging than that in the uplink where multiuser signals can be separated by the massive MIMO at the BS. While massive MIMO can most certainly use its super-high spatial resolution to provide directional, focused signals onto the RIS, the finer separation of multiuser signals towards the target UEs requires complex optimization of the reflection coefficients of the meta-atoms on the RIS. Note that different from traditional multiuser MIMO beamforming, the same set of reflection coefficients is used to direct the radio signals of all the UEs. This indeed limits the ability of RIS to resolve the UE signals in the spatial domain. Therefore, recent interest is seen to shift more responsibility to the UEs and non-orthogonal multiple access (NOMA) emerges to be one possible solution [145], [146]. Scalability, however, can be a real problem as UEs usually have limited processing capability, not to mention the complexity associated with user pairing and coordinating all the CSI for carrying out effective interference cancellation at the receiving UEs.

With FAMA, multiuser communications can be achieved by skimming through the fading envelopes observed in the space of the fluid antenna at each UE and tuning to operate at the position where the interference is in a deep fade, without the need for complex coordination and signal processing. Consider the case that an N_T-antenna BS communicates to $N_{\text{I}}+1$ fluid-antenna UEs via an RIS with M reflecting elements. Then the received signal at the k-th port of the fluid antenna at UE m can be written in a standard FAMA form as

$$y_k^{(m)} = g_k^{(m)} s_m + \tilde{g}_k^{(m)} + \eta_k^{(m)}, \quad (32)$$

in which s_m denotes the information-bearing modulated signal for UE m, $\eta_k^{(m)}$ is the additive white Gaussian noise (AWGN)

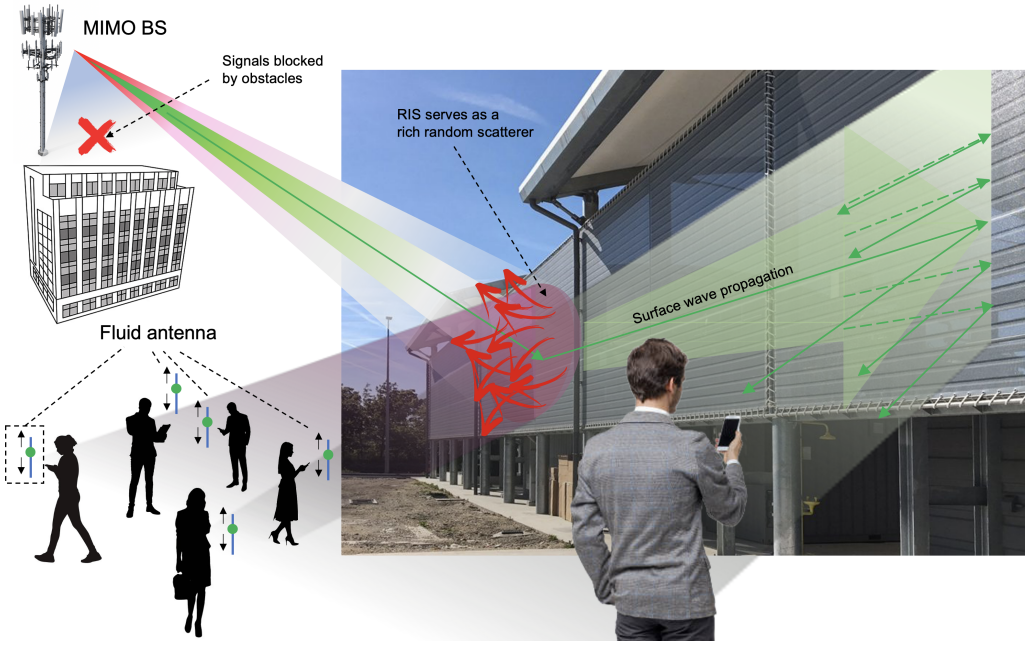

Fig. 16. MIMO, RIS and fluid antennas all combine to provide mobile communications from the BS to several UEs via a RIS.

at the k-th port of UE m, and according to [147],

$$g_k^{(m)} = \mathbf{h}_{\text{RIS-UE},(m,k)}^{\dagger} \boldsymbol{\Upsilon} \mathbf{H}_{\text{BS-RIS}} \mathbf{f}_m, \tag{33}$$

$$\tilde{g}_k^{(m)} = \mathbf{h}_{\text{RIS-UE},(m,k)}^{\dagger} \boldsymbol{\Upsilon} \mathbf{H}_{\text{BS-RIS}} \sum_{\substack{\ell=1 \\ \ell \neq m}}^{N_{\text{I}}+1} \mathbf{f}_\ell s_\ell, \tag{34}$$

where $\mathbf{h}_{\text{RIS-UE},(m,k)} \in \mathbb{C}^{M \times 1}$ is the channel vector from the RIS to UE m at port k, $\mathbf{H}_{\text{BS-RIS}} \in \mathbb{C}^{M \times N_T}$ denotes the channel matrix from the BS to the RIS, $\boldsymbol{\Upsilon}$ denotes a diagonal matrix containing the phase shifts of all the meta-atoms, and $\mathbf{f}_\ell \in \mathbb{C}^{N_T \times 1}$ is the precoding vector at the BS for UE ℓ. Note that $\tilde{g}_k^{(m)}$ is the symbol-level aggregate interference signal.

For FAMA to work, the only requirement is that $g_k^{(m)}$ and $\tilde{g}_k^{(m)}$ should have independent channel envelopes, which can be ensured by properly choosing the precoding vectors $\{\mathbf{f}_\ell\}$. One sensible choice would be the singular-value decomposition (SVD) subspaces of $\mathbf{H}_{\text{BS-RIS}}$ which can not only deliver strong signal beams from the BS to the RIS but also provide sufficient independency of the multiuser signals reaching the RIS. The burden to optimize $\boldsymbol{\Upsilon}$ is much reduced because the RIS mainly acts as a massive scatterer and if M is large, then both $g_k^{(m)}$ and $\tilde{g}_k^{(m)}$ will be Gaussian distributed regardless of the choice of $\boldsymbol{\Upsilon}$. This implies that a random choice of $\boldsymbol{\Upsilon}$ is sufficient and the complexity for acquiring and coordinating the CSI between the RIS and UEs as well as optimizing $\boldsymbol{\Upsilon}$ can be avoided, yet enabling massive multiple access for the UEs if the number of ports at each UE is large enough.

B. Exploiting Normal and Tangential Radio Waves on RIS

As discussed in [56], RIS exploiting surface wave communications can offer exciting opportunities to localize mobile connections and considerably simplify interference management. This advantage also comes with the fact that the propagation characteristics on the surface remains more or less the same over a wide bandwidth, meaning that the optimized surface wave pathways for the UEs work naturally even if multi-carrier modulation such as OFDM is used. Same cannot be said for conventional RIS since multipath reacts differently at different frequencies and yet there is only one single $\boldsymbol{\Upsilon}$ to strengthen the links between the RIS and the UEs at all frequencies.

A more natural reason to exploit surface wave communications is probably that radio waves coming from the BS arrive the RIS at a natural incident angle which means that they have normal and tangential components to the surface. Therefore, the natural tangential component of the radio waves makes the surface wave that can be guided by the RIS with appropriate meta-atom designs. Note that the whole idea of optimizing $\boldsymbol{\Upsilon}$ for RIS is to reassemble all the radio waves captured by the large surface aperture and redirect them towards the UEs. This is evidently not easy especially when interference is part of the signals from the RIS to UEs. Beamforming from the RIS is also limited by the phase shifting range of the meta-atoms and its inability to independently control the amplitude of the reflection coefficients. Though the normal component of the radio waves naturally bounces off the surface like what an RIS expects, collecting the tangential component and keeping it on the surface will greatly improve the aperture efficiency of the RIS to generate more useful signals to the UEs.

In addition, with FAMA in mind, the choice of $\boldsymbol{\Upsilon}$ does not matter and the meta-atoms can be solely optimized to create surface wave pathways for routing the radio signals before the signals are diffracted off the surface. Remarkably, all is done without concerning how the mixed signals are resolved at the UE side as this is taken care of by the fluid antennas.

Most importantly, using surface wave communications on RIS might be the only option for wideband communications. According to [148], a well-designed microstrip-like meta-atom

at 4GHz has only about 500MHz bandwidth where there is a maximum of 1.25π phase shift range (much less than 2π) and the amplitude fluctuation is less than 4dB. Worse, at 4.5GHz, the phase shift range falls to only π. This practically means that the promises of an ideally-optimized $\boldsymbol{\Upsilon}$ are not realistic. The narrow operating bandwidth of conventional RIS will be a major bottleneck for high-speed communications from the BS to the UEs if reflection-based RIS is to be relied on. By contrast, a surface wave platform can be made to have a very stable performance over an extremely wide bandwidth (e.g., 52GHz in [101]). As a consequence, the tangential component of the radio waves (or surface waves) on the RIS may be the only useful signals that are left to exploit in wideband communications. Note also that the bandwidth of RIS can be significantly increased if the amplitude fluctuation and phase shift range of the meta-atoms do not matter, as will be the case when RIS serves merely as a massive, randomized scatterer for fluid antennas to exploit at the UE side.

C. Scalability and Compatibility

As discussed above, the objective of RIS is to act as a large aperture for capturing as much useful radio signals as possible by serving as a massive RIS scatterer as well as exploiting the surface waves, while fluid antennas at the UEs are responsible for resolving the interference at the UEs. Multiple RISs thus can coexist without the need for careful planning, coordination and optimization. This is not the case if RIS is employed as a beamformer because the generated interference needs to be coordinated. In the RIS-FAMA paradigm, however, more RISs certainly improve the system performance because they collect more radio energy and the increase in the number of scattering elements will help deepen the fade, providing more ups and downs in the fading envelopes seen by fluid antennas. Network scalability over the number of UEs is also high. A desirable phenomenon is that the more the number of coexisting UEs, the deeper the fade, suggesting that the number of UEs does not adversely affect the interference immunity of a FAMA UE though the overall interference power in general tends to increase with the number of coexisting UEs. In the same spirit, no coordination between BSs is needed if an RIS is being used for serving edge-of-cell UEs in multicell scenarios.

The above is possible because FAMA is entirely user-centric and requires no coordination between BSs, RISs and UEs. The processing at a FAMA UE also has no impact on coexisting UEs. The interference suppression capability comes naturally from the fading phenomenon. Moreover, the interference immunity comes without requiring any side information of the interferers, which makes it particularly appealing.

VI. Conclusions

The numerous exciting opportunities and experience mobile communications is giving us, continue to push our technology to new heights. While MIMO has been instrumental to unlock the needed bandwidth to take mobile communications to where we are, this paper serves to look beyond MIMO and discuss two emerging technologies that can be combined with MIMO. The first part of the paper introduced the first technology, namely RIS which includes the conventional reflection-based RIS as a special case (including both passive and active/semi-active RIS). Different from the literature, we also include the surface-wave enabled RIS which can serve as a propagation medium as well as a reflector to enjoy much superior propagation efficiency, reconfigurable pathways and highly localized mobile connections. We covered the basics of surface waves and reviewed how the surface meta-atoms can be optimized to meet various communication needs. The second part then presented another key technology, fluid antennas that represent a novel, position-and-shape changeable antenna architecture for ultimate reconfigurability. We outlined the basic antenna architecture and reviewed two relevant fluid antenna designs that are important for beyond 5G systems. We also highlighted a few theoretical results that revealed the immense diversity and capacity gains possible for systems utilizing fluid antennas. We concluded this paper by contemplating the scenario in which MIMO, RIS and fluid antennas all combine to deliver mobile communications and highlighted their synergies.

In summary, we pointed out that

- Multiuser MIMO at the BS can be most effective to direct its signals to RISs to reach the target UEs. The BS should be responsible for ensuring channel independency among users for the signals coming onto the RIS.
- The use of FAMA eliminates the need of optimizing the reflection coefficients of the meta-atoms while benefiting from the large number of scattering elements on the RIS to produce the needed fading fluctuations to be exploited by fluid antennas at the UEs for multiple access.
- The union of RIS and FAMA removes any processing and messaging requirements at the RIS for CSI acquisition and managing multiuser detection at the UEs.
- RIS using surface waves to capture the tangential radio energy to the surface may be the only feasible solution for wideband communications due to the narrow bandwidth of the state-of-the-art RIS meta-atom technology.
- Surface waves can lead to superior propagation efficiency and ease interference management. The optimization for surface wave pathways is also relatively straightforward and requires only the location information of the UEs. The technology for switching between surface and space waves to connect the UEs is already available.
- The overall approach is compatible in multicell environments and scales well with any number of RISs. FAMA works well with any number of coexisting UEs as long as the resolution of the fluid antennas is high enough.

It is hoped that the opportunities discussed in this paper can spark further interest and research efforts in the related areas, which can pave the way for 6G mobile communications.

References

[1] M. H. Miraz, M. Ali, P. S. Excell and R. Picking, "A review on Internet of Things (IoT), Internet of Everything (IoE) and Internet of Nano Things (IoNT)," in Proc. *Internet Technol. and Appl.*, pp. 219–224, 8-11 Sept. 2015, Wrexham, UK.

[2] G. P. Fettweis, "The tactile internet: Applications and challenges," *IEEE Veh. Technol. Mag.*, vol. 9, no. 1, pp. 64–70, Mar. 2014.

[3] W. Shi, J. Cao, Q. Zhang, Y. Li and L. Xu, "Edge computing: Vision and challenges," *IEEE Internet of Things J.*, vol. 3, no. 5, pp. 637–646, Oct. 2016.

[4] X. Lu, P. Wang, D. Niyato, D. I. Kim and Z. Han, "Wireless networks with RF energy harvesting: A contemporary survey," *IEEE Commun. Surveys & Tutorials*, vol. 17, no. 2, pp. 757–789, 2015.

[5] R. Molina-Masegosa and J. Gozalvez, "LTE-V for sidelink 5G V2X vehicular communications: A new 5G technology for short-range vehicle-to-everything communications," *IEEE Veh. Technol. Mag.*, vol. 12, no. 4, pp. 30–39, Dec. 2017.

[6] F. Tariq *et al.*, "A speculative study on 6G," *IEEE Wireless Commun.*, vol. 27, no. 4, pp. 118–125, Aug. 2020.

[7] A. J. Paulraj, and T. Kailath, "Increasing capacity in wireless broadcast systems using distributed transmission/directional reception (DTDR)," *US Patent 5,345,599A*, granted 1994.

[8] G. J. Foschini, and M. J. Gans, "On limits of wireless communications in a fading environment when using multiple antennas," *Wireless Pers. Commun.*, vol. 6, no. 3, pp. 311–335, Mar. 1998.

[9] V. Tarokh, N. Seshadri, and A. R. Calderbank, "Space-time codes for high data rate wireless communication: Performance criterion and code construction," *IEEE Trans. Inform. Theory*, vol. 44, no. 2, pp. 744–765, Mar. 1998.

[10] S. M. Alamouti, "A simple transmit diversity technique for wireless communications," *IEEE J. Select. Areas Commun.*, vol. 16, no. 8, pp. 1451–1458, Oct. 1998.

[11] L. Zheng, and D. N. C. Tse, "Diversity and multiplexing: A fundamental tradeoff in multiple-antenna channels," *IEEE Trans. Inform. Theory*, vol. 49, no. 5, pp. 1073–1096, May 2003.

[12] K. K. Wong, R. D. Murch, R. S. K. Cheng and K. B. Letaief, "Optimizing the spectral efficiency of multiuser MIMO smart antenna systems," in *Proc. IEEE Wireless Commun. Netw. Conf.*, vol. 1, pp. 426–430, 23-28 Sep. 2000, Chicago, IL, USA.

[13] K. K. Wong, R. D. Murch and K. B. Letaief, "A joint-channel diagonalization for multiuser MIMO antenna systems," *IEEE Trans. Wireless Commun.*, vol. 2, no. 4, pp. 773–786, Jul. 2003.

[14] S. Vishwanath, N. Jindal, and A. Goldsmith, "Duality, achievable rates, and sum-rate capacity of Gaussian MIMO broadcast channels," *IEEE Trans. Inform. Theory*, vol. 49, no. 10, pp. 2658–2668, Oct. 2003.

[15] Q. H. Spencer, A. L. Swindlehurst, and M. Haardt, "Zero-forcing methods for downlink spatial multiplexing in multiuser MIMO channels," *IEEE Trans. Signal Proc.*, vol. 52, no. 2, pp. 461–471, Feb. 2004.

[16] D. Gesbert, M. Kountouris, R. W. Heath, C. Chae and T. Salzer, "Shifting the MIMO paradigm," *IEEE Sig. Proc. Mag.*, vol. 24, no. 5, pp. 36–46, Sep. 2007.

[17] D. J. Love *et al.*, "An overview of limited feedback in wireless communication systems," *IEEE J. Select. Areas Commun.*, vol. 26, no. 8, pp. 1341–1365, Oct. 2008.

[18] A. Alkhateeb, O. El Ayach, G. Leus and R. W. Heath, "Channel estimation and hybrid precoding for millimeter wave cellular systems," *IEEE J. Select. Topics Sig. Proc.*, vol. 8, no. 5, pp. 831–846, Oct. 2014.

[19] S. Han, C. I, Z. Xu and C. Rowell, "Large-scale antenna systems with hybrid analog and digital beamforming for millimeter wave 5G," *IEEE Commun. Mag.*, vol. 53, no. 1, pp. 186–194, Jan. 2015.

[20] F. Sohrabi and W. Yu, "Hybrid digital and analog beamforming design for large-scale antenna arrays," *IEEE J. Select. Topics Sig. Proc.*, vol. 10, no. 3, pp. 501–513, Apr. 2016.

[21] H. Q. Ngo, E. G. Larsson, and T. L. Marzetta, "Energy and spectral efficiency of very large multiuser MIMO systems," *IEEE Trans. Commun.*, vol. 61, no. 4, pp. 1436–1449, Apr. 2013.

[22] E. G. Larsson, O. Edfors, F. Tufvesson, and T. L. Marzetta, "Massive MIMO for next generation wireless systems," *IEEE Commun. Mag.*, vol. 52, no. 2, pp. 186–195, Feb. 2014.

[23] Z. Chang, L. Lei, Z. Zhou, S. Mao, and T. Ristaniemi, "Learn to cache: Machine learning for network edge caching in the big data era," *IEEE Wireless Commun.*, vol. 25, no. 3, pp. 28–35, Jun. 2018.

[24] R. Romana, J. Lopez, and M. Mambo, "Mobile edge computing, fog *et al.*: A survey and analysis of security threats and challenges," *Future Generation Computer Systems*, vol. 78, pp. 680–698, 2018.

[25] C. Liaskos *et al.*, "A new wireless communication paradigm through software-controlled metasurfaces," *IEEE Commun. Mag.*, vol. 56, no. 9, pp. 162–169, Sep. 2018.

[26] E. Basar *et al.*, "Wireless communications through reconfigurable intelligent surfaces," *IEEE Access*, vol. 7, pp. 116753–116773, 2019.

[27] M. Di Renzo *et al.*, "Smart radio environments empowered by reconfigurable AI meta-surfaces: An idea whose time has come," *EURASIP J. Wireless Commun. and Netw.*, vol. 2019, no. 129, 2019.

[28] S. Hu, F. Rusek and O. Edfors, "Beyond massive MIMO: The potential of data transmission with large intelligent surfaces," *IEEE Trans. Sig. Proc.*, vol. 66, no. 10, pp. 2746–2758, May 2018.

[29] W. Tang *et al.*, "A programmable metasurface based RF chain-free 8PSK wireless transmitter," *IET Elect. Letters*, vol. 55, no. 7, pp. 417–420, Apr. 2019.

[30] W. Tang *et al.*, "MIMO transmission through reconfigurable intelligent surface: System design, analysis, and implementation," *IEEE J. Select. Areas Commun.*, vol. 38, no. 11, pp. 2683–2699, Nov. 2020.

[31] Industry Specification Group (ISG) on Reconfigurable Intelligent Surfaces (RIS). [Online]. Available: https://www.etsi.org/committee/1966-ris?jjj=1631218280300.

[32] S. Abadal, T. Cui, T. Low, and J. Georgiou, "Programmable metamaterials for software-defined electromagnetic control: Circuits, systems, and architectures," *IEEE J. Emerging and Select. Topics Circuits and Systems*, vol. 10, no. 1, pp. 6–19, Mar. 2020.

[33] L. Dai *et al.*, "Reconfigurable intelligent surface-based wireless communications: Antenna design, prototyping, and experimental results," *IEEE Access*, vol. 8, pp. 45913-45923, Mar. 2020.

[34] R. W. Ziolkowski and A. Erentok, "Metamaterial-based efficient electrically small antennas," *IEEE Trans. Antennas and Propag.*, vol. 54, no. 7, pp. 2113–2130, Jul. 2006.

[35] Y. Dong and T. Itoh, "Metamaterial-based antennas," *Proc. IEEE*, vol. 100, no. 7, pp. 2271–2285, Jul. 2012.

[36] G. L. Stüber, *Principles of Mobile Communication*, Second Edition, Kluwer Academic Publishers, 2002.

[37] E. Björnson and L. Sanguinetti, "Rayleigh fading modeling and channel hardening for reconfigurable intelligent surfaces," *IEEE Wireless Commun. Letters*, vol. 10, no. 4, pp. 830–834, Apr. 2021.

[38] K. K. Wong, A. Shojaeifard, K. F. Tong, and Y. Zhang, "Performance limits of fluid antenna systems," *IEEE Commun. Letters*, vol. 24, no. 11, pp. 2469–2472, Nov. 2020.

[39] K. K. Wong, A. Shojaeifard, K. F. Tong, and Y. Zhang, "Fluid antenna systems," *IEEE Trans. Wireless Commun.*, vol. 20, no. 3, pp. 1950–1962, Mar. 2021.

[40] K. K. Wong, K. F. Tong, Y. Zhang, and Z. Zheng, "Fluid antenna system for 6G: When Bruce Lee inspires wireless communications," *IET Elect. Letters*, vol. 56, no. 24, pp. 1288–1290, Nov. 2020.

[41] D. Rodrigo, B. A. Cetiner and L. Jofre, "Frequency, radiation pattern and polarization reconfigurable antenna using a parasitic pixel layer," *IEEE Trans. Antennas & Propag.*, vol. 62, no. 6, pp. 3422–3427, Jun. 2014.

[42] S. Song and R. D. Murch, "An efficient approach for optimizing frequency reconfigurable pixel antennas using genetic algorithms," *IEEE Trans. Antennas & Propag.*, vol. 62, no. 2, pp. 609–620, Feb. 2014.

[43] S. J. Kar, A. Chakrabarty and B. K. Sarkar, "Fluid antennas," in *Proc. IEEE Middle East Conf. Antennas and Propag. (MECAP 2010)*, pp. 1–6, 20-22 Oct. 2010, Cairo, Egypt.

[44] C. Borda-Fortuny, L. Cai, K. F. Tong, and K. K. Wong, "Low cost 3D-printed coupling-fed frequency agile fluidic monopole antenna system," *IEEE Access*, vol. 7, pp. 95058–95064, Jul. 2019.

[45] C. B. Fortuny, K. F. Tong, A. Al-Armaghany, and K. K. Wong, "A low-cost fluid switch for frequency-reconfigurable Vivaldi antenna," *IEEE Antennas and Wireless Propag. Letters*, vol. 16, pp. 3151–3154, Nov. 2017.

[46] A. Singh, I. Goode and C. E. Saavedra, "A multistate frequency reconfigurable monopole antenna using fluidic channels," *IEEE Antennas and Wireless Propag. Letters*, vol. 18, no. 5, pp. 856–860, May 2019.

[47] G. J. Hayes, J. So, A. Qusba, M. D. Dickey and G. Lazzi, "Flexible liquid metal alloy (EGaIn) microstrip patch antenna," *IEEE Trans. Antennas and Propag.*, vol. 60, no. 5, pp. 2151–2156, May 2012.

[48] A. M. Morishita, C. K. Y. Kitamura, A. T. Ohta and W. A. Shiroma, "A liquid-metal monopole array with tunable frequency, gain, and beam steering," *IEEE Antennas and Wireless Propag. Letters*, vol. 12, pp. 1388–1391, 2013.

[49] A. Dey, R. Guldiken and G. Mumcu, "Microfluidically reconfigured wideband frequency-tunable liquid-metal monopole antenna," *IEEE Trans. Antennas and Propag.*, vol. 64, no. 6, pp. 2572–2576, Jun. 2016.

[50] Y. Huang, L. Xing, C. Song, S. Wang and F. Elhouni, "Liquid antennas: Past, present and future," *IEEE Open J. Antennas and Propag.*, vol. 2, pp. 473–487, 2021.

[51] "Mitsubishi electric's SeaAerial antenna uses seawater plume," Available [online]: https://www.mitsubishielectric.com.

[52] M. Hampson, "New antenna uses saltwater and plastic to steer radio beams," *IEEE Spectrum-The Tech Talk blog*, 2019.

[53] L. Xing, J. Zhu, Q. Xu, D. Yan and Y. Zhao, "A circular beam-steering antenna with parasitic water reflectors," *IEEE Antennas and Wireless Propag. Letters*, vol. 18, no. 10, pp. 2140–2144, Oct. 2019.

[54] J. Kimionis, A. Georgiadis, A. Collado, and M. M. Tentzeris, "Enhancement of RF tag backscatter efficiency with low-power reflection

amplifiers," *IEEE Trans. Microw. Theory Technol.*, vol. 62, no. 12, pp. 3562–3571, Oct. 2014.

[55] E. Basar and H. V. Poor, "Present and future of reconfigurable intelligent surface-empowered communications," 2021. [Online]. Available: https://arxiv.org/abs/2105.00671.

[56] K. K. Wong, K. F. Tong, Z. Chu and Y. Zhang, "A vision to smart radio environment: Surface wave communication superhighways," *IEEE Wireless Commun.*, vol. 28, no. 1, pp. 112–119, Feb. 2021.

[57] H. M. Barlow and A. L. Cullen, "Surface waves," *J. Inst. Electr. Eng.*, vol. 1953, no. 11, pp. 363–364, Nov. 1953.

[58] W. Tang *et al.*, "Wireless communications with reconfigurable intelligent surface: Path loss modeling and experimental measurement," *IEEE Trans. Wireless Commun.*, vol. 20, no. 1, pp. 421–439, Jan. 2021.

[59] Z. Chu, K. K. Wong and K. F. Tong, "Reconfigurable surface wave platform using fluidic conductive structures," in *Proc. IEEE Int. Symp. Antennas and Prop. and USNC-URSI Radio Science Meeting (AP-S/URSI 2021)*, 4-10 Dec. 2021, Marina Bay Sands, Singapore.

[60] J. Y. Dai *et al.*, "High-efficiency synthesizer for spatial waves based on space-time-coding digital metasurface," *Laser & Photonics Rev.*, vol. 14, no. 6, pp. 190033, Jun. 2020.

[61] J. Y. Dai *et al.*, "Wireless communication based on information meta-surfaces," *IEEE Trans. Micro. Theory and Tech.*, vol. 69, no. 3, pp. 1493–1510, Mar. 2021.

[62] N. T. Nguyen, J. He, V.-D. Nguyen, H. Wymeersch, D. W. K. Ng, R. Schober, S. Chatzinotas, and M. Juntti, "Hybrid relay-reflecting intelligent surface-aided wireless communications: Opportunities, challenges, and future perspectives," 2021. [Online]. Available: https://arxiv.org/abs/2104.02039.

[63] N. T. Nguyen, Q.-D. Vu, K. Lee, and M. Juntti, "Spectral efficiency optimization for hybrid relay-reflecting intelligent surface," in *Proc. IEEE Int. Conf. Commun. Workshop*, 2021. [Online]. Available: https://arxiv.org/abs/2105.00345.

[64] N. T. Nguyen, Q.-D. Vu, K. Lee, and M. Juntti, "Hybrid relay-reflecting intelligent surface-assisted wireless communication," 2021. [Online]. Available: https://arxiv.org/abs/2103.03900.

[65] Q. Wu and R. Zhang, "Intelligent reflecting surface enhanced wireless network: Joint active and passive beamforming design," in *Proc. IEEE Global Commun. Conf.*, 9-13 Dec. 2018, United Arab Emirates.

[66] Q. Wu and R. Zhang, "Intelligent reflecting surface enhanced wireless network via joint active and passive beamforming," *IEEE Trans. Wireless Commun.*, vol. 18, no. 11, pp. 5394–5409, Aug. 2019.

[67] Q. Wu and R. Zhang, "Beamforming optimization for wireless network aided by intelligent reflecting surface with discrete phase shifts," *IEEE Trans. Wireless Commun.*, vol. 68, no. 3, pp. 1838–1851, Dec. 2019.

[68] S. Abeywickrama, R. Zhang, Q. Wu, and C. Yuen, "Intelligent reflecting surface: Practical phase shift model and beamforming optimization," *IEEE Trans. Commun.*, vol. 68, no. 9, pp. 5849–5863, Jun. 2020.

[69] S. Zhang and R. Zhang, "Capacity characterization for intelligent reflecting surface aided MIMO communication," *IEEE J. Sel. Areas Commun.*, vol. 38, no. 8, pp. 1823–1838, Jun. 2020.

[70] N. S. Perović, L.-N. Tran, M. Di Renzo, and M. F. Flanagan, "Achievable rate optimization for MIMO systems with reconfigurable intelligent surfaces," *IEEE Trans. Wireless Commun.*, vol. 20, no. 6, pp. 3865–3882, Feb. 2021.

[71] B. Ning, Z. Chen, W. Chen, and J. Fang, "Beamforming optimization for intelligent reflecting surface assisted MIMO: A sum-path-gain maximization approach," *IEEE Wireless Commun. Lett.*, vol. 9, no. 7, pp. 1105–1109, Mar. 2020.

[72] Y. Zhang, C. Zhong, Z. Zhang, and W. Lu, "Sum rate optimization for two way communications with intelligent reflecting surface," *IEEE Commun. Lett.*, vol. 24, no. 5, pp. 1090–1094, Mar. 2020.

[73] C. Pan, H. Ren, K. Wang, W. Xu, M. Elkashlan, A. Nallanathan, and L. Hanzo, "Multicell MIMO communications relying on intelligent reflecting surfaces," *IEEE Trans. Wireless Commun.*, vol. 19, no. 8, pp. 5218–5233, May 2020.

[74] L. Yang, Y. Yang, D. B. da Costa, and I. Trigui, "Outage probability and capacity scaling law of multiple RIS-aided networks," *IEEE Wireless Commun. Lett.*, vol. 10, no. 2, pp. 256–260, Sep. 2020.

[75] P. Wang, J. Fang, X. Yuan, Z. Chen, and H. Li, "Intelligent reflecting surface-assisted millimeter wave communications: Joint active and passive precoding design," *IEEE Trans. Veh. Technol.*, vol. 69, no. 12, pp. 14 960–14 973, Oct. 2020.

[76] N. S. Perović, L.-N. Tran, M. D. Renzo and M. F. Flanagan, "Optimization of RIS-aided MIMO systems via the cutoff rate," *IEEE Wireless Commun. Letters*, vol. 10, no. 8, pp. 1692–1696, Aug. 2021.

[77] Y. Zhang, B. Di, H. Zhang, J. Lin, C. Xu, D. Zhang, Y. Li, and L. Song, "Beyond cell-free MIMO: Energy efficient reconfigurable intelligent surface aided cell-free MIMO communications," *IEEE Trans. Cogn. Commun. Netw.*, vol. 7, no. 2, pp. 412–426, Feb. 2021.

[78] S. Huang, Y. Ye, M. Xiao, H. V. Poor, and M. Skoglund, "Decentralized beamforming design for intelligent reflecting surface-enhanced cell-free networks," *IEEE Commun. Lett.*, vol. 10, no. 3, pp. 673–677, Dec. 2020.

[79] R. Long, Y.-C. Liang, Y. Pei, and E. G. Larsson, "Active reconfigurable intelligent surface aided wireless communications," *IEEE Trans. Wireless Commun.*, Mar. 2021, early access.

[80] W. Shi, X. Zhou, L. Jia, Y. Wu, F. Shu and J. Wang, "Enhanced secure wireless information and power transfer via intelligent reflecting surface," *IEEE Commun. Letters*, vol. 25, no. 4, pp. 1084–1088, Apr. 2021.

[81] D. Mishra and H. Johansson, "Channel estimation and low-complexity beamforming design for passive intelligent surface assisted MISO wireless energy transfer," in *Proc. IEEE Int. Conf. Acoustics, Speech and Sig. Process. (ICASSP)*, pp. 4659–4663, 12-17 May 2019, Brighton, UK.

[82] K. Ardah, S. Gherekhloo, A. L. F. de Almeida, and M. Haardt, "TRICE: An efficient channel estimation framework for RIS-Aided MIMO communications," *IEEE Signal Process. Lett.*, vol. 28, pp. 513–517, Feb. 2021.

[83] J. He, H. Wymeersch, and M. Juntti, "Channel estimation for RIS-aided mmWave MIMO systems via atomic norm minimization," *IEEE Trans. Wireless Commun.*, 2021, early access.

[84] J. Mirza and B. Ali, "Channel estimation method and phase shift design for reconfigurable intelligent surface assisted MIMO networks," *IEEE Trans. Cogn. Commun. Netw.*, vol. 7, no. 2, pp. 441–451, Jun. 2021.

[85] G. T. de Araújo, A. L. De Almeida, and R. Boyer, "Channel estimation for intelligent reflecting surface assisted MIMO systems: A tensor modeling approach," *IEEE J. Sel. Areas Commun.*, vol. 15, no. 3, pp. 789–802, Feb. 2021.

[86] A. Taha, M. Alrabeiah, and A. Alkhateeb, "Enabling large intelligent surfaces with compressive sensing and deep learning," *IEEE Access*, vol. 9, pp. 44 304–44 321, Mar. 2021.

[87] J. He, M. Leinonen, H. Wymeersch and M. Juntti, "Channel estimation for RIS-aided mmWave MIMO systems," in *Proc. IEEE Global Commun. Conf. (GLOBECOM)*, pp. 1–6, 7-11 Dec. 2020, Taipei, Taiwan.

[88] G. C. Alexandropoulos and E. Vlachos, "A hardware architecture for reconfigurable intelligent surfaces with minimal active elements for explicit channel estimation," in *Proc. IEEE Int. Conf. Acoustics, Speech and Signal Process. (ICASSP)*, pp. 9175–9179, 4-8 May 2020, Barcelona, Spain.

[89] R. Schroeder, J. He, and M. Juntti, "Passive RIS vs. Hybrid RIS: A comparative study on channel estimation," in *Proc. IEEE Veh. Technol. Conf. (VTC2021-Spring)*, 25-28 Apr. 2021, Helsinki, Finland.

[90] Y. Lin, S. Jin, M. Matthaiou, and X. You, "Tensor-Based algebraic channel estimation for hybrid IRS-Assisted MIMO-OFDM," *IEEE Trans. Wireless Commun.*, vol. 20, no. 6, pp. 3770–3784, Jan. 2021.

[91] G. C. Alexandropoulos, N. Shlezinger, I. Alamzadeh, M. F. Imani, H. Zhang, and Y. C. Eldar, "Hybrid reconfigurable intelligent meta-surfaces: Enabling simultaneous tunable reflections and sensing for 6G wireless communications," 2021. [Online]. Available: https://arxiv.org/abs/2104.04690.

[92] F. Rusek, D. Persson, B. K. Lau, E. G. Larsson, T. L. Marzetta, O. Edfors, and F. Tufvesson, "Scaling up MIMO: Opportunities and challenges with very large arrays," *IEEE Signal Process. Mag.*, vol. 30, no. 1, pp. 40–60, 2012.

[93] H. Q. Ngo, A. Ashikhmin, H. Yang, E. G. Larsson, and T. L. Marzetta, "Cell-free massive MIMO versus small cells,"' *IEEE Trans. Wireless Commun.*, vol. 16, no. 3, pp. 1834–1850, 2017.

[94] L. Liu and W. Yu, "Massive connectivity with massive MIMO–Part I: Device activity detection and channel estimation," *IEEE Trans. Signal Process.*, vol. 66, no. 11, pp. 2933–2946, 2018.

[95] H. Q. Ngo, L.-N. Tran, T. Q. Duong, M. Matthaiou, and E. G. Larsson, "On the total energy efficiency of cell-free massive MIMO," *IEEE Trans. Green Commun. Network.*, vol. 2, no. 1, pp. 25–39, 2017.

[96] J. He, K. Yu, Y. Shi, Y. Zhou, W. Chen, and K. B. Letaief, "Reconfigurable intelligent surface assisted massive MIMO with antenna selection," *IEEE Trans. Wireless Commun.*, 2021, early access.

[97] K. Zhi, C. Pan, H. Ren, and K. Wang, "Ergodic rate analysis of reconfigurable intelligent surface-aided massive MIMO systems with ZF detectors," *IEEE Commun. Lett.*, 2021, early access.

[98] N. T. Nguyen, V.-D. Nguyen, V.-H. Nguyen, H. Q. Ngo, S. Chatzinotas, and M. Juntti, "Downlink throughput of cell-free massive MIMO systems assisted by hybrid relay-reflecting intelligent surfaces," in *Proc. IEEE Int. Conf. Commun. (ICC)*, 2022, submitted.

[99] C. Burrows, "Existence of a surface wave in radio propagation," *Nature*, vol. 138, pp. 284, 1936.

[100] T. K. Sarkar, M. N. Abdallah, M. Salazar-Palma and W. M. Dyab, "Surface plasmons-polaritons, surface waves, and Zenneck waves: Clarification of the terms and a description of the concepts and their evolution," *IEEE Antennas and Propag. Mag.*, vol. 59, no. 3, pp. 77–93, Jun. 2017.

[101] J. Wan, K. F. Tong and C. H. Chan, "Simulation and experimental verification for a 52 GHz wideband trapped surface wave propagation system," *IEEE Trans. Antennas and Propag.*, vol. 67, no. 4, pp. 2158–2166, Apr. 2019.

[102] K. F. Tong, J. X. Wan, X. D. Wang and C. B. Wu, "On the gain and link equation for reactive millimetre-wave surface wave propagation system," in Proc. *IEEE Asia-Pacific Conf. Antennas and Propag. (APCAP)*, pp. 425-428, 5-8 Aug. 2018, Auckland, New Zealand.

[103] J. Wan, K. F. Tong and C. Wu, "The excitation efficiency of surface waves on a reactive surface by a finite vertical aperture," in Proc. *IEEE Int. Symp. Antennas and Propag. & USNC/URSI National Radio Science Meeting*, pp. 1634–1635, 19-24 Jul. 2015, Vancouver, BC, Canada.

[104] A. Kay and F. Zucker, "Efficiency of surface wave excitation," *IRE Int. Convention Record*, pp. 1–5, 21-25 Mar. 1966, New York, NY, USA.

[105] H. M. Barlow, and B. John, *Radio surface waves*, Oxford, Clarendon Press, 1962.

[106] B. Zheng and R. Zhang, "Intelligent reflecting surface-enhanced OFDM: Channel estimation and reflection optimization," *IEEE Wireless Commun. Letters*, vol. 9, no. 4, pp. 518–522, Apr. 2020.

[107] Z. Wang, L. Liu and S. Cui, "Channel estimation for intelligent reflecting surface assisted multiuser communications: Framework, algorithms, and analysis," *IEEE Trans. Wireless Commun.*, vol. 19, no. 10, pp. 6607–6620, Oct. 2020.

[108] V. S. Asadchy, M. Albooyeh, S. N. Tcvetkova, A. Daz-Rubio, Y. Ra'di, and S. A. Tretyakov, "Perfect control of reflection and refraction using spatially dispersive metasurfaces," *Phys. Rev. B*, vol. 94, no. 7, pp. 075142, Aug. 2016.

[109] A. A. Fathnan, A. Olk, and D. Powell, "Broadband anomalous reflection with dispersion controlled metasurfaces," *arXiv Appl. Phys.*, 2019

[110] A. Sutinjo and M. Okoniewski, "A surface wave holographic antenna for broadside radiation excited by a traveling wave patch array," *IEEE Trans. Antennas Propag.*, vol. 59, no. 1, pp. 297–300, Jan. 2011.

[111] S. K. Podilchak, L. Matekovits, A. P. Freundorfer, Y. M. M. Antar, and M. Orefice, "Controlled leaky-wave radiation from a planar configuration of width-modulated microstrip lines," *IEEE Trans. Antennas Propag.*, vol. 61, no. 10, pp. 4957–4972, Oct. 2013.

[112] H. H. Lv, Q. L. Huang, J. L. Liu, J. Q. Hou, and X. W. Shi, "Holographic design of beam-switchable leaky-wave antenna," *IEEE Antennas Wirel. Propag. Lett.*, vol. 18, no. 12, pp. 2736–2740, Dec. 2019.

[113] M. ElSherbiny, A. E. Fathy, A. Rosen, G. Ayers, and S. M. Perlow, "Holographic antenna concept, analysis, and parameters," *IEEE Trans. Antennas Propag.*, vol. 52, no. 3, pp. 830–839, Mar. 2004.

[114] T. Zhao, D. R. Jackson, J. T. Williams, H. Y. D. Yang, and A. A. Oliner, "2-D periodic leaky-wave antennas – Part I: Metal patch design," *IEEE Trans. Antennas Propag.*, vol. 53, no. 11, pp. 3505–3514, Nov. 2005.

[115] T. Zhao, D. R. Jackson, J. T. Williams, and A. A. Oliner, "General formulas for 2-D leaky-wave antennas," *IEEE Trans. Antennas Propag.*, vol. 53, no. 11, pp. 3525–3533, Nov. 2005.

[116] Z. Chu, K. K. Wong and K. F. Tong, "Enhancing and localizing surface wave propagation with reconfigurable surfaces," in *Proc. IEEE Int. Symp. Antennas & Propag. (ISAP)*, pp. 1–2, 19-22 Oct. 2021, Taipei, Taiwan.

[117] Z. Gao *et al.*, "Surface-wave pulse routing around sharp right angles," *Phys. Rev. Appl.*, vol. 9, no. 4, pp. 044019, Apr. 2018.

[118] J. Costantine, Y. Tawk, S. E. Barbin, and C. G. Christodoulou, "Reconfigurable antennas: Design and applications," *Proc. IEEE*, vol. 103, no. 3, pp. 424–437, Mar. 2015.

[119] N. Ojaroudi Parchin *et al.*, "Recent developments of reconfigurable antennas for current and future wireless communication systems," *Electronics*, vol. 8, no. 2, pp. 128, Jan. 2019.

[120] L. Xing *et al.*, "Further investigation on water antennas," *IET Microwaves & Antennas Propag.*, vol. 9, pp. 735–741, 2015.

[121] R. J. Espley-Jones, K. F. Tong, J. E. J. Dalley and J. D. S. Langley, "Demonstrating a low temperature organic dense dielectric patch antenna," in *Proc. Loughborough Antennas & Propag. Conf. (LAPC 2017)*, 13-14 Nov. 2017, Loughborough, UK.

[122] Y. Li and K.-M. Luk, "A water dense dielectric patch antenna," *IEEE Access*, vol. 3, pp. 274–280, Apr. 2015.

[123] E. Motovilova and S. Y. Huang, "A review on reconfigurable liquid dielectric antennas," *Materials (Basel).*, vol. 13, no. 8, pp. 1863, Apr. 2020.

[124] S. Keyrouz, and D. Caratelli, "Dielectric resonator antennas: Basic concepts, design guidelines, and recent developments at millimeter-wave frequencies," *Int. J. Antennas & Propag.*, vol. 2016.

[125] A. Petosa, A. Ittipiboon, Y. M. M. Antar, D. Roscoe and M. Cuhaci, "Recent advances in dielectric-resonator antenna technology," *IEEE Antennas & Propag. Mag.*, vol. 40, no. 3, pp. 35–48, Jun. 1998.

[126] M. Cosker, L. Lizzi, F. Ferrero, R. Staraj and J. Ribero, "Realization of 3-D flexible antennas using liquid metal and additive printing technologies," *IEEE Antennas & Wireless Propag. Letters*, vol. 16, pp. 971–974, Oct. 2017.

[127] W. Su, S. A. Nauroze, B. Ryan and M. M. Tentzeris, "Novel 3D printed liquid-metal-alloy microfluidics-based zigzag and helical antennas for origami reconfigurable antenna 'trees'," in *Proc. 2017 IEEE MTT-S Int. Microwave Symp. (IMS)*, pp. 1579–1582, 4-9 Jun. 2017, Honolulu, HI, USA.

[128] Y.-N. Wang and L.-M. Fu, "Micropumps and biomedical applications – A review," *Microelectron. Eng.*, vol. 195, pp. 121–138, Aug. 2018.

[129] S. G. Darby *et al.*, "A metering rotary nanopump for microfluidic systems," *Lab Chip*, vol. 10, no. 23, pp. 3218–3226, 2010.

[130] S. Haykin, "Cognitive radio: Brain-empowered wireless communications," *IEEE J. Select. Areas Commun.*, vol. 23, no. 2, pp. 201–220, Feb. 2005.

[131] J. Mitola and G. Q. Maguire, "Cognitive radio: Making software radios more personal," *IEEE Pers. Commun.*, vol. 6, no. 4, pp. 13–18, Aug. 1999.

[132] Y. Shen, K. F. Tong, and K. K. Wong, "Beam-steering surface wave fluid antennas for MIMO applications," in *Proc. The 2020 Asia-Pacific Microwave Conf. (APMC 2020)*, pp. 634–636, 8-11 Dec. 2020, Hong Kong SAR, China.

[133] C. Xu, Y. Wang, J. Wu, and Z. Wang, "Parasitic circular patch antenna with continuously tunable linear polarization using liquid metal alloy," *Microw. Opt. Technol. Lett.*, vol. 61, no. 3, pp. 727–733, Mar. 2019.

[134] Y.-H. Qian and Q.-X. Chu, "A pattern-reconfigurable water-loaded MIMO antenna," *Microw. Opt. Technol. Lett.*, vol. 59, no. 7, pp. 1608–1613, Jul. 2017.

[135] M. D. Dickey *et al.*, "Eutectic Gallium-Indium (EGaIn): A liquid metal alloy for the formation of stable structures in microchannels at room temperature," *Adv. Funct. Mater.*, vol. 18, no. 7, pp. 1097–1104, Apr. 2008.

[136] P. Geddis, L. Wu, A. McDonald, S. Chen, and B. Clements, "Effect of static liquid Galinstan on common metals and non-metals at temperatures up to 200°C," *Can. J. Chem.*, vol. 98, no. 12, pp. 787–798, Dec. 2020.

[137] L. Xing, Y. Huang, Q. Xu, S. Alja'afreh and T. Liu, "Complex permittivity of water-based liquids for liquid antennas," *IEEE Antennas & Wireless Propag. Letters*, vol. 15, pp. 1626–1629, 2016.

[138] Z. Chen and H. Wong, "Liquid dielectric resonator antenna with circular polarization reconfigurability," *IEEE Trans. Antennas and Propag.*, vol. 66, no. 1, pp. 444–449, Jan. 2018.

[139] Z. Chen and H. Wong, "Wideband glass and liquid cylindrical dielectric resonator antenna for pattern reconfigurable design," *IEEE Trans. Antennas and Propag.*, vol. 65, no. 5, pp. 2157–2164, May 2017.

[140] M. Konca and P. A. Warr, "A frequency-reconfigurable antenna architecture using dielectric fluids," *IEEE Trans. Antennas and Propag.*, vol. 63, no. 12, pp. 5280–5286, Dec. 2015.

[141] S. Wang, L. Zhu and W. Wu, "A novel frequency-reconfigurable patch antenna using low-loss transformer oil," *IEEE Trans. Antennas and Propag.*, vol. 65, no. 12, pp. 7316–7321, Dec. 2017.

[142] K. K. Wong, K. F. Tong, Y. Chen and Y. Zhang, "Closed-form expressions for spatial correlation parameters for performance analysis of fluid antenna systems," to appear in *IET Electronics Letters*, 2022.

[143] K. K. Wong and K. F. Tong, "Fluid antenna multiple access," to appear in *IEEE Trans. Wireless Commun.*, 2022, early access.

[144] Z. Chai, K. K. Wong, K. F. Tong, Y. Chen and Y. Zhang, "Port selection for fluid antenna systems," to appear in *IEEE Commun. Letters*, 2022, early access.

[145] Z. Ding and H. Vincent Poor, "A simple design of IRS-NOMA transmission," *IEEE Commun. Letters*, vol. 24, no. 5, pp. 1119–1123, May 2020.

[146] B. Zheng, Q. Wu and R. Zhang, "Intelligent reflecting surface-assisted multiple access with user pairing: NOMA or OMA?," *IEEE Commun. Letters*, vol. 24, no. 4, pp. 753–757, Apr. 2020.

[147] H. U. Rehman, F. Bellili, A. Mezghani and E. Hossain, "Joint active and passive beamforming design for IRS-assisted multi-user MIMO systems: A VAMP-based approach," to appear in *IEEE Trans. Commun.*, 2021.

[148] J. Y. Dai *et al.*, "Wireless communications through a simplified architecture based on time-domain digital coding metasurface," *Adv. Materials Technol.*, vol. 4, no. 7, Feb. 2019.